For submission after AE review and revision to Earth Surface Processes and Landforms as a Research Article

Thursday, August 18, 2016

Rates of erosion and landscape change along the Blue Ridge escarpment, southern Appalachian Mountains, estimated from *in situ* cosmogenic ^{10}Be

Colleen L. Linari

Geology Department, University of Vermont, Burlington, Vermont 05405, USA

Paul R. Bierman*

Geology Department and School of Natural Resources, University of Vermont, Burlington, Vermont 05405, USA

Eric W. Portenga

Department of Earth and Environmental Sciences, University of Michigan, Ann Arbor, Michigan 48109, USA

Milan J. Pavich

U.S. Geological Survey, Reston, Virginia 20192, USA

Robert C. Finkel

Department of Earth and Planetary Sciences, University of California, Berkeley, CA 95064, USA and Center for Accelerator Mass Spectrometry, Lawrence Livermore National Laboratory, Livermore, CA 94550, USA

Stewart P.H.T. Freeman

SUERC Accelerator Mass Spectrometry Laboratory, East Kilbride, Scotland

*Corresponding author: e-mail: pbierman@uvm.edu
phone: 802-656-4411, fax: 802-656-0045

Keywords: Beryllium-10, passive margin, cosmogenic isotopes

Abstract

The Blue Ridge escarpment, located within the southern Appalachian Mountains of Virginia and North Carolina, forms a distinct, steep boundary between the lower-elevation Piedmont and higher-elevation Blue Ridge physiographic provinces. To understand better the rate at which this landform and the adjacent landscape are changing, we measured cosmogenic ^{10}Be in quartz separated from sediment samples (n = 50) collected in thirty-two streams and from three exposed bedrock outcrops along four transects normal to the escarpment, allowing us to calculate erosion rates integrated over 10^4–10^5 years. These basin-averaged erosion rates (5.4–49 m My^{-1}) are consistent with those measured elsewhere in the southern Appalachians and show a positive relationship between erosion rate and average basin slope. Erosion rates show no relationship with basin size or relative position of the Brevard fault zone, a fundamental structural element of the region. The cosmogenic isotopic data, when considered along with the distribution of average basin slopes in each physiographic province, suggest that the escarpment is eroding on average more rapidly than the Blue Ridge uplands, which are eroding more rapidly than the Piedmont lowlands. This difference in erosion rates by geomorphic

setting suggests that the elevation difference between the uplands and lowlands adjacent to the escarpment is being reduced but at extremely slow rates.

Introduction

Great escarpments associated with extensional tectonics exist on nearly all continents and are located along active and recently rifted margins as well as along older margins (Matmon et al., 2002; Spotila et al., 2004). Such escarpments have been extensively studied in terms of the climatic, tectonic, and geomorphic processes that shape them (Cockburn et al., 2000; Gilchrist and Summerfield, 1990; Heimsath et al., 2006; Mandal et al., 2015; Matmon et al., 2002; Ollier, 1984; Persano et al., 2002; Salgado et al., 2013; Scharf et al., 2013; Seidl et al., 1996; Spotila et al., 2004; Summerfield et al., 1997; Tucker and Slingerland, 1994).

The Blue Ridge escarpment, located inland of the passive margin of eastern North America (Figure 1), is a unique feature of the southern Appalachian Mountains characterized by its linear trend, its steep slopes (~20° to 30°), and a dramatic elevation change over only a few kilometers. The escarpment is sub-parallel to the Atlantic margin and is a distinct topographic boundary between the lower-elevation Piedmont and higher-elevation Blue Ridge physiographic provinces (Figure 2). The escarpment forms an asymmetric drainage divide where streams flowing to the Gulf of Mexico have to travel six times the distance (3000 km) of those flowing to the Atlantic Ocean (Figure 1;

Dietrich, 1959; Spotila et al., 2004). The escarpment and surrounding landscapes are generally underlain by micaceous schist and gneiss, although locally they are underlain by granitic rocks and quartz-rich graywackes; thus, the escarpment's morphology cannot be attributed to differences in the bedrock's resistance to erosion (Hack, 1982; Spotila et al., 2004).

Passive margin escarpments are often the result of uplift from rifting, and rift basin boundary faults are often assumed to generate such escarpments. Following the cessation of active rifting, escarpments are shaped by erosional processes that in general cause escarpments to retreat (backwear) from the faults. Great escarpments are found either along continental rifts representing early stages of crustal extension, or inland of passive margins representing later stages (Matmon et al., 2002). Although it is generally agreed that rift escarpments are formed tectonically by normal faulting and maintained by erosion, alternative hypotheses have been advanced to explain how they change over time after rifting ceases (Japsen et al., 2012; Spotila et al., 2004). The original paradigm (Ollier, 1984). suggested ongoing, significant, and parallel escarpment retreat over time. More recent thinking, based largely on geochronologic data, suggests rapid and significant erosion only during the earliest stages of extension followed by the development of a stable or very slowly eroding passive margin escarpment (Spotila et al., 2004; Bierman and Caffee, 2001; Heimsath et al., 2006; Matmon et al., 2002; Seidl et al., 1996; Tucker and Slingerland, 1994; Vanacker et al., 2007).

The Blue Ridge escarpment is smaller, more discontinuous, and on a much older passive margin than most other rift-generated great escarpments, having formed more than 200 million years ago (Heimsath et al., 2006; Seidl et al., 1996; Bierman and Caffee, 2001; Brown et al., 2000; Fleming et al., 1999; Heimsath et al., 2006; Ollier, 1984; Persano et al., 2002; Spotila et al., 2004; Summerfield et al., 1997). Yet, more than 200 My after collisional orogenic events ceased and rifting from Africa terminated (Schlische, 1993), the Appalachians in general, and the Blue Ridge escarpment in particular, still exhibit considerable relief (Davis, 1899; Hack, 1960; Rowley et al., 2013; Miller et al., 2013).

The erosional history and development of the Blue Ridge escarpment have been extensively studied but remain incompletely understood although multiple lines of evidence suggest at least some and perhaps significant control on the overall surface morphology by tectonic and/or mantle processes (Battiau-Queney, 1989; Davis, 1903; Dietrich, 1957, 1959; Hack, 1982; Pazzaglia and Brandon, 1996; Pazzaglia and Gardner, 1994; Spotila et al., 2004; Tucker and Slingerland, 1994; White, 1950). Seismic data suggest that the high topography of the escarpment is underlain by a thick root of low-density continental crust while the adjacent lowlands are underlain by denser material (Pratt et al., 1988; Wagner et al., 2012). Seismic data suggest tens of millions of years ago a hidden hotspot may have passed through northern Virginia although the effect of such a passage on escarpment topography is uncertain (Chu et al., 2013). Field

observations as well as numerical landscape analysis and modeling suggest that the area around the escarpment is significantly and episodically modified by drainage capture events and large scale recent uplift (dynamic topography) likely driven by mantle processes (Prince et al., 2010, 2011; Prince and Spotila, 2013; Gallen et al., 2013; Rowley et al., 2013; Schmandt and Lin, 2014; Miller et al., 2013; Naeser et al., 2016). Such capture events transiently increase the rate of basin-scale erosion and escarpment retreat in specific areas along escarpment strike as base-level falls rapidly and incision propagates upstream.

Erosion rates calculated from measured concentrations of cosmogenic nuclides such as ^{10}Be quantify the rate of landscape change on a 10^4–10^5-year time scale and consequently can also quantify the tempo of passive margin escarpment retreat on a time scale integrated over cyclic Quaternary climate changes (Heimsath et al., 2006; Bierman and Caffee, 2001). Such data, in conjunction with data from geochronometers such as fission track and (U-Th)/He thermochronology, which integrate over longer time frames (~10^8 years; e.g., Spotila et al., 2004; Brown et al., 2000; McKeon et al., 2011), allow for the testing of theories of long-term landscape evolution. For example, if thermochronologic data show no time-distance relationship across the lowlands and cosmogenic data indicate millennial-timescale rates of retreat for an inland escarpment that are too slow to accommodate the distance the escarpment has moved over the time interval since rifting began, then the concept of an escarpment continuously retreating at

one rate over time is not plausible. In such a case, the erosion responsible for the inland position of the escarpment either must have occurred rapidly, soon after rifting, such that a period of relative erosional stability (post retreat) coincides with the integration time of the thermochronologic data or that the erosion occurs episodically, through drainage capture and rapid back-wearing of drainage divides (Prince et al., 2010, 2011; Prince and Spotila, 2013).

Here we use measurements of *in situ* produced cosmogenic ^{10}Be in fluvial sediment to estimate millennial-scale erosion rates and test the hypothesis that the Blue Ridge escarpment is actively retreating by determining whether there are statistically different rates of denudation between the Blue Ridge highlands (the upland), the Piedmont (the lowland), and the escarpment zone (steep topography) that could lead to changing relief and escarpment position over time. To gain a better understanding of landscape change in and near the Blue Ridge escarpment and the southern Appalachian Mountains, we consider the hypotheses that erosion rates are correlative with basin slope and landscape position. By understanding the behavior of the Blue Ridge escarpment over time and space, our data contribute to a better understanding of passive margin escarpments in general although we recognize that the integration time of ^{10}Be in stable, passive margin environments (tens of thousands to a few hundred thousand years) does not allow us to address large-scale, long-term landscape changes definitively with this new data set.

Background

Southern Appalachian Mountains

The Appalachian Mountains formed during a series of Paleozoic collisional tectonic events culminating with the cessation of the Permian Alleghenian Orogeny. Erosion during the Permian and early Triassic was followed by continental rifting and rift margin uplift in the Mesozoic associated with the opening of the Atlantic Ocean at ~200 Ma. Numerous rift basins formed via normal faulting on the central Atlantic margin of North America during the initial extensional events that separated North America and Africa (Schlische, 1993). The western-most Mesozoic rift basin, the Dan River-Danville basin, is ~35 km east of a section of the Blue Ridge escarpment (Spotila et al., 2004), and represents the closest mapped normal boundary fault to the escarpment (Figure 1), and thus a minimum distance for escarpment retreat. Other basins, further to the east, would suggest even greater retreat distances.

After rift shoulder uplift associated with the onset of continental extension ceased, denudation and isostatic compensation have prevailed throughout the range (Judson, 1975; Pazzaglia and Brandon, 1996; Schlische, 1993; Slingerland and Furlong, 1989; Matmon et al., 2003). Several datasets suggest that erosion and thus sediment delivery from the range has likely not been steady over time scales of 10^6–10^8 years. For example, Pazzaglia and Brandon (1996) show large changes over the last 10^8 years in rates of

sediment delivery to the passive margin, Prince et al. (2010, 2011) and Prince and Spotila (2013) argue that drainage capture leads to rapid downcutting and consequent landscape change over 10^6 year timescales, and Naeser et al. (2016) provide thermochronologic evidence for a major Miocene dranage capture event. Modeling (Rowley et al., 2013) supported by mantle imaging (Schmandt and Lin, 2014) suggest that some Appalachian topography (on the scale of 10^2 meters of uplift) is dynamically supported and quite young, 10^6 years. The influence of this dynamic topography is revealed in the Appalachian landscape by knickzones incising headward as the landscape uplifts (Miller et al., 2013).

The southern Appalachian Mountains in the area near the Blue Ridge escarpment have a humid temperate climate. A major portion of the region's abundant precipitation (~1,100–1,500 mm yr^{-1}) occurs during the warmest periods, usually during a few severe storm events (http://www.sercc.com/; accessed January 2007; Dietrich, 1959). At elevation, freeze and thaw cycles make frost cracking a potentially important weathering agent (Matsuoka and Murton, 2008). The study area has not been glaciated (Barron, 1988; Richmond and Fullerton, 1986) although the climate was considerably colder than today and periglacial processes operated at high elevations during the Pleistocene glacial maxima (Delcourt and Delcourt, 1984).

The topography of the Appalachian Mountains is less rugged than that of active mountain belts; however, the orogenic crustal root beneath the mountain chain is still

relatively thick (40–50 km) and more typical of much higher mountain ranges (Baldwin et al., 2003; Matmon et al., 2003; Pratt et al., 1988; Wagner et al., 2012). However, the climate is too warm to support glaciation and the rapid erosion it causes, and together with the lack of tectonic activity, relief is much less than in active mountain ranges. It is not clear whether relief is stable or changing today; however, erosion could lead to relief production by increasing valley erosion rates relative to summit lowering rates (Hancock and Kirwan, 2007; Portenga et al., 2013). Relief production could be caused in the absence of tectonic forcing by drainage capture (Prince et al., 2010, 2011; Prince and Spotila, 2013) and by uplift induced by dynamic topography (Miller et al., 2013) although the timescales of these phenomena far exceed the integration time of ^{10}Be in fluvial sediment which records a 10^4–10^5 year record of landscape erosion.

The Brevard fault zone is a major regional structure (Figure 1) that is oriented southwest-northeast and extends for ~600 km from Alabama to Virginia (Figure 1; Roper and Justus, 1973). The Brevard fault zone was active during the Taconic and Acadian orogenies, well before the rifting events that formed the Blue Ridge escarpment. In some places, it is coincident with the boundary between the Blue Ridge and Piedmont provinces but the Brevard fault zone only coincides with the Blue Ridge escarpment for 50–60 km. It deviates from the escarpment both to the northeast, where it is farther east in the Piedmont, and to the southwest, where it is within the Blue Ridge Mountains (Hack, 1982; Roper and Justus, 1973).

A mixture of second growth deciduous forest and fields cleared for agriculture covers the basins we sampled in this study. Most of the landscape is soil-mantled and there is saprolite exposed in road and stream cuts. Active surface processes that move sediment down slopes and into channels include tree throw, stream bank erosion, and gully erosion. Most physical erosion and sediment transport are likely caused by soil creep, mass wasting, and the action of running water (cf., Jungers et al., 2009). Debris flows may affect the steepest terrain (Witt et al., 2007), primarily on the escarpment although, we saw no recent debris flow paths or run outs during our fieldwork.

Blue Ridge Escarpment Erosion

Many hypotheses have been advanced in an attempt to explain the evolution of the Blue Ridge escarpment (Davis, 1903; Dietrich, 1957; Hack, 1982; Hayes and Campbell, 1894; Ollier, 1984; Pazzaglia and Gardner, 1994; Spotila et al., 2004; White, 1950). Hayes and Campbell (1894) suggested that monoclinal flexure formed the Blue Ridge escarpment. As asymmetrical uplift took place on the upland, stream erosion on the Piedmont accelerated and moved headward creating the scarp (Dietrich, 1959; Hack, 1982). Later, Davis (1903) suggested that the escarpment developed as a result of the position of the regional drainage divide (Davis, 1903; Hack, 1982; Spotila et al., 2004). Davis argued that streams flowing to the Atlantic had an advantage over streams flowing to the Gulf of Mexico because they had a shorter distance to travel. This hypothesis was

disputed by Hack (1982), who noted that western rivers descend to the low continental interior over a similar distance before flowing to the Gulf of Mexico. Building on Davis' model, Dietrich (1957) proposed that the escarpment was formed by erosion accompanying westward migration of the asymmetric drainage divide (Bank, 2002; Dietrich, 1957). Hack (1975) additionally proposed that the highlands west of the escarpment have persisted due to resistant sandstones and quartzites, which set the base level for westward draining streams (Bank, 2002; Hack, 1975; Spotila et al., 2004).

White (1950) introduced the hypothesis that the scarp was produced by local, normal-sense reactivation of a fault within the Brevard fault zone during the Mesozoic (Dietrich, 1957; Hack, 1982; Spotila et al., 2004). His theory was based on diffuse shear planes and aligned bedrock schistosity (Spotila et al., 2004; White, 1950). Evidence for tectonic rejuvenation has been criticized (Dietrich, 1957), because the Brevard fault zone only coincides with the escarpment for 50–60 km (Hack, 1982; Roper and Justus, 1973).

Rift-flank uplift followed by parallel slope retreat is a concept commonly applied to great escarpments. Uplift occurs along a rift axis, creating an escarpment and asymmetric drainage divide, and topography is maintained as the divide migrates away from the rift margin (Ollier, 1984; Spotila et al., 2004). This hypothesis has only been briefly considered for the Blue Ridge escarpment (Ollier, 1984). Pazzaglia and Gardner (1994) proposed that flexural isostasy was responsible for creating the Blue Ridge escarpment. They suggested that as the Appalachian Mountains eroded, sediment was

carried to the coast and deposited offshore, causing local subsidence of the middle Atlantic margin and flexural rebound inland of the area of subsidence. They propose a positive feedback in which erosion drives isostatic uplift which in turn causes more erosion, with continued westward migration of the escarpment over time (Bank, 2002; Pazzaglia and Gardner, 1994; Spotila et al., 2004). Recent work suggests dynamic solid Earth processes may be influencing Appalachian topography (e.g., Rowley et al., 2013).

Cosmogenic nuclides in erosion studies

In situ-produced cosmogenic nuclides such as ^{10}Be are produced in materials at or near Earth's surface as cosmic rays interact with minerals such as quartz in rock and sediment (Lal, 1991) and have provided erosion rate data for passive margin escarpments worldwide (e.g., Bierman and Caffee, 2001; Cockburn et al., 1999; Fleming et al., 1999; Heimsath et al., 2006; Seidl et al., 1996; Vanacker et al., 2007; Matmon et al., 2013). This technique has also been used elsewhere in the Appalachian Mountains to evaluate erosion rates at both the outcrop and basin scale (Hancock and Kirwan, 2007; Matmon et al., 2003; Portenga et al., 2013; Duxbury et al., 2015; Reusser et al., 2015). Cosmogenic nuclide analysis has proven to be a useful tool for understanding geologic rates of surface change and bedrock erosion because the penetration depth of cosmic rays causes nuclide concentrations in sediment to average erosion rates over the time period required to erode ~60 cm of rock or more than a meter of soil, thereby buffering the impact of both human-

induced and naturally-forced episodic erosion (Brown et al., 1998; Kirchner et al., 2001; Hewawasam et al., 2003; Reusser et al., 2015). Numerous studies have shown that the mixing of soil and regolith by physical and biological processes minimizes the effect of land-use change and consequent erosion on the concentration of cosmogenic nuclides in sediment and thus the calculation of long-term erosion rates (e.g., Hewawasam et al., 2003; Jungers et al., 2009). Thus, even though the area we sampled has been used for timber harvesting and agriculture, the long term erosion rates we calculate are likely representative of erosion rates integrated over tens of thousands of years including significant climate changes between glacial and interglacial times.

Methods

We collected fluvial sediment samples from streams draining 32 basins. We selected basins suitable for sampling using GIS and a 30 m SRTM digital elevation model (earthexplorer.usgs.gov) to determine basin size, average basin slope, and physiographic province after which, we verified basin access using 1:24,000 USGS topographic maps. Rather than sampling randomly, we sampled locations that represented a variety of basin sizes and slopes within each physiographic province in an effort to investigate factors that may influence erosion rates. The sediment samples were collected from four transects, each normal to the escarpment, separated by ~320 km (Figure 1). Two transects were situated at the southern end of the escarpment, one where the Brevard

fault zone is completely within the Blue Ridge province, and the other where the fault zone coincides with the escarpment. The remaining two transects were located along the northern end of the escarpment where the Brevard zone is seaward of the escarpment, completely within the Piedmont province. We sampled three bedrock outcrops; in this soil-mantled landscape such outcrops were rare. These outcrops were ~1 m higher than the surrounding soil cover, and samples were collected from the upper flat surface of the outcrops. Bedrock sample thicknesses (for each sample) averaged 3 cm.

We collected fluvial sediment from streambeds (bars and shallow pools) and recorded the location of each sampling site (Figure 1, Table 1). We sieved six samples from Transect C into four grain size fractions: 0.25–0.85 mm, 0.85–2.0 mm, 2.0–9.0 mm, and >9.0 mm to test whether a relationship exists between sediment grain size and ^{10}Be concentration. Grain size fractions larger than 0.85 mm were ground and sieved to 0.25–0.85 mm and each sample was processed individually. For all other samples (n = 26), we processed only the 0.25–0.85 mm fraction. Bedrock samples (n = 3) were ground to sand-size particles for processing. We isolated quartz (11–41 g) using the method of Kohl and Nishiizumi (1992).

All but six samples were prepared at the University of Vermont using techniques outlined in Bierman and Caffee (2002). In each batch of samples, there were seven unknowns and one full process blank (SPEX 1000 ppm ICP standard). The ^{10}Be isolated from these samples was analyzed using accelerator mass spectrometry (AMS) at the

Lawrence Livermore National Laboratory (LLNL). The average ratio of the ten Vermont process blanks was subtracted from the measured ^{10}Be ratios. Measured ratios for samples analyzed at LLNL were normalized using the KNSTD3110 standard assuming a ^{10}Be/^{9}Be ratio for the standard of 3.15 x 10^{-12}.

Samples CS-11, -12, and -17 and replicates of samples CS-14, -24, and -30 were processed at the Scottish Universities Environmental Research Centre (SUERC) (http://www.gla.ac.uk/suerc/index.html) in East Kilbride, Scotland following procedures based on methods modified from Kohl and Nishiizumi (1992) and Child et al. (2000), at the GU-SUERC Cosmogenic Isotope Laboratory. The ^{10}Be isolated in Scotland was measured at the SUERC Accelerator Mass Spectrometry Laboratory (Xu et al., 2015). Blank correction was done on the basis of one blank processed with these samples. The samples analyzed at SUERC were normalized using the standard NIST (SRM4325) (National Institute of Standards and Technology) assuming a ^{10}Be/^{9}Be ratio for the standard of 3.06 x 10^{-11}, analogous to the original value of the KNSTD standard series prior to the recent recalculation of the ^{10}Be half-life (Nishiizumi et al., 2007).

In general replicates agreed well (R^2 = 0.97); two of the three replicates agree within the 1σ analytic uncertainties of the measurements, a reassuring finding considering that the Be was extracted in two different laboratories by different people using different methods and that isotopic ratios were measured on different accelerators and normalized to different standards. In statistical analyses and for plotting data, we use

the average of replicates. To determine the uncertainty of this average, we use a conservative approach and report the larger of (1) the standard deviation of that average or (2) the average AMS analytical uncertainty of the two measurements. Uncertainties reported for all nuclide concentrations include the 1σ AMS measurement uncertainty with fully propagated blank uncertainty. Blank correction amounts to at most a few percent, and usually much less of the measured sample ratios.

We calculated effective elevations and latitudes for each basin (cf., Portenga and Bierman, 2011), allowing the cosmogenic production rate of each basin to be summarized as a single point in space. Erosion rates (Bierman and Steig, 1996) were calculated with these results and isotopic data using the CRONUS on-line calculator (Balco et al., 2008, version 2.2, Lal/Stone scaling, global production rate) taking into account the different standards used for AMS normalization (Table 2).

We used regression models and a series of one-way analysis of variance tests to check for relationships between the isotopic data (erosion rates) and basin-specific characteristics such as average basin slope, basin area, and landscape position.

We classified the geographic location of each sample by considering whether a majority of the drainage basin was located in either the Blue Ridge (upland) or Piedmont (lowland) physiographic province or on the steep escarpment zone (Figure 1, Table 1). For this study, we specified the escarpment zone on the basis of slopes derived from digital elevation models (30 m resolution). We quantitatively delineated the heart of the

escarpment zone by identifying high-slope cells that were surrounded by a majority of cells with slopes >15° within a 500 m radius. Setting the threshold for what we considered to be high-slopes any lower resulted in large areas of both Piedmont and Blue Ridge upland surfaces being incorporated into the escarpment zone. We drew a 1,000 m buffer around the delineated escarpment zone to create one conterminous geographical unit, which includes the upper and lower transitions of the escarpment zone with the Blue Ridge and Piedmont provinces, respectively. We consider the escarpment zone's western border (the eastern boundary of the Blue Ridge uplands) to be the Mississippi River Basin drainage divide; the escarpment zone's eastern border (the western boundary of the Piedmont) is defined by the limits of the 1,000 m buffer. Relief for each catchment (Table 1) is the difference between the highest point of each catchment and the sample collection site elevation.

Because we could only sample a limited number of drainage basins across the region for erosion rate determination with ^{10}Be, we must consider how representative the sampled basins are of the surrounding landscape as a whole, specifically in regards to slope which is in many studies (including this one) is well correlated to erosion rate (Portenga and Bierman, 2011). In other words, we seek to test whether the basins we sampled were representative of the physiographic provinces in which they were located and that determine whether our sampling was biased in terms of average basin slope.

To characterize physical differences between the three physiographic provinces in which we collected samples, we subdivided a swath of the landscape (including the Blue Ridge upland, the escarpment zone, and the Piedmont lowland) encompassing the four sampled transects, into constituent tributary drainage basins (average area = 14.1 ± 4.1 km^2, median area = 14.3 km^2, n = 1,084) using ArcGIS. During basin delineation, the average basin area was set in ArcGIS to approximate that of the basins that were actually sampled (average =10.7 ± 17.6 km^2, median = 5.0 km^2, n = 32). We assigned each resultant sub-basin to the Blue Ridge (upland), escarpment, or Piedmont (lowland) based upon which province the majority of the sub-basin area fell within (Table 3). Because the escarpment covers only a narrow zone of the landscape, some delineated escarpment basins include headwaters that originate on the lower relief Blue Ridge upland province. Similarly, for some lowland Piedmont basins, small portions of the lower escarpment may contribute sediment to the drainage basin. Using summary statistics for each sub-basin, we constructed cumulative probability density functions showing the distribution of mean slopes for all sub-basins within a given province (shown as insets in Figure 6).

Using the relationship between mean basin slope and erosion rate derived from our cosmogenic isotope analysis (Figure 3), we estimated synthetic rates of erosion for each of the delineated 1,084 sub-basins based only on average basin slope using the erosion rate/slope regression analysis appropriate for each physiographic province. Based upon the mean slopes of all GIS-delineated basins in each of the three provinces, and the

relative area of each basin, we calculated area-weighted model erosion rates for the Blue Ridge, the escarpment, and the Piedmont provinces in their entirety (Table 3). We stress that these are synthetic rates based on the relationship of average basin slope to erosion rate calculated from our sampling of the basin populations defined in GIS. Making these calculations is an important correction to our data because it accounts for sampling bias in terms of average basin slope.

Results

Nuclide Concentrations and Measured Erosion Rates

Fluvial samples from on and near the Blue Ridge escarpment contain 1.21–11.1 x 10^5 atoms g^{-1} of ^{10}Be (Table 2). Considering only the 0.25–0.85 mm grain size fraction data from all transects, sediment samples from the Blue Ridge province (n = 10) have an average erosion rate of 13.8 m My^{-1}. Those basins draining only the escarpment (n = 20) yield an average erosion rate of 21.9 m My^{-1}. Fluvial sediment samples from the Piedmont province (n = 2) yield an average erosion rate of 12.2 m My^{-1} (Table 3).

Landscape-erosion rate relationships

Using bivariate regression analyses, slope emerged as the only significant landscape parameter related to erosion (Figures 3, 4, 5). In general, basins with steeper slopes have higher erosion rates than basins with gentler slopes (Figure 3) as has been

found elsewhere (Montgomery and Brandon, 2002; Portenga and Bierman, 2011). For the entire dataset, there is a positive relationship between average basin slope and erosion rate.

Erosion rate (m My^{-1}) = slope (°) * 1.53 - 0.98, $R^2 = 0.54$, $p < 0.0001$

Note that there is a negative intercept which appears to be the result of a robust slope/erosion rate relationship with basins that have $>10^o$ mean slope and no dependence on slope for erosion rates in basins where average basin slope is $< 10^o$. In those low slope basins, erosion rates are similar, ranging between 8 and 14 m/My.

This slope-erosion rate relationship also holds true for basins sampled in the Blue Ridge province ($R^2 = 0.52$) and for escarpment basins ($R^2 = 0.46$). There are only two Piedmont samples in this study. The predictive power of the erosion rate-slope relationship in the overall dataset is moderate; however, when average basin slope of basins sampled per province is considered with respect to average erosion rate per province, the relationship becomes much more powerful ($R^2 = 0.99$; inset of Figure 3). There is no significant relationship between erosion rate and basin area or with basin elevation when the entire dataset is considered (Figures 4, 5).

Drainage basin slope distribution analysis

Because average basin slope and erosion rate are correlated, it is important to know the slope distribution of drainage basins within each physiographic province to evaluate whether the samples we collected are in fact representative of the subpopulations of all the basins within each province (see methods section for rationale). Using GIS analysis, we found the average slope of all small basins (~14.1 km^2) within the Blue Ridge province (the uplands) is 13.3 ± 4.3° (n = 447). All small basins within the escarpment yield an average slope of 14.3 ± 2.6° (n = 145) and all small basins within the Piedmont province (lowlands) yield an average slope of 6.2 ± 2.7° (n = 492). These province-averaged slopes are similar to the average slopes of the basins we sampled for two of the three provinces (Escarpment 14.3° vs. 15.1°; Piedmont 6.2° vs. 7.7°) but quite different for the Blue Ridge, 13.3° vs. 9.6°. Thus, we conclude that our sampling from the Blue Ridge was biased. Our samples are not representative of the province-averaged population in terms of average basin slope; we collected samples biased toward low-slope basins and thus the average erosion rate we calculate for the Blue Ridge province is too low. This is shown graphically by the clustering of Blue Ridge province samples at low average basin slopes (Figure 6).

The dependence of erosion rate on slope allows us to calculate a synthetic erosion rate for each province in order to correct any bias in our sampling. Using linear regression, we present the following models for erosion rate of the three provinces we define in this paper:

Blue Ridge erosion rate (m My^{-1}) = slope (°) * 1.132 + 2.933, R^2 = 0.52, *n* = 10

Escarpment erosion rate (m My^{-1}) = slope (°) * 1.959 - 7.666, R^2 = 0.46, *n* = 20

Piedmont erosion rate (m My^{-1}) = slope (°) * 1.060 + 4.015, R^2 = 1.0, *n* = 2

Using the average basin slope data for all basins in the three provinces, we calculate the average province erosion rates in various ways (Table 3). It is important to note that no matter which way we calculate province-specific erosion rates, the escarpment is eroding more quickly than the Blue Ridge (uplands), which erodes more quickly than the Piedmont (lowlands).

Grain-size specific nuclide concentration

Nuclide concentration data for the six samples in which multiple grain sizes were analyzed separately (CS-01, CS-02, CS-03, CS-04, CS-06, CS-07) show no consistent pattern of nuclide concentration and grain size (Figure 7). Because of this and for consistency, we calculate erosion rates only for the 0.25 to 0.85 mm grain size. Only one of these six samples (CS-07) shows a monotonic decrease of ^{10}Be concentration with increasing grain size. In four samples (CS-01, CS-02, CS-03, CS-06) the largest grain

size yields the highest ^{10}Be concentration, with no systematic pattern between smaller grain sizes. The remaining sample (CS-04) exhibits no systematic relationship among grain sizes. Integrating the results for all grain sizes of all six samples, no statistically significant relationship exists between ^{10}Be concentrations and grain size ($F_{3, 20} = 0.246$, $p = 0.86$).

Bedrock erosion rates for samples collected from outcrops on and near the escarpment were highly variable: 106 m My^{-1} (CSB-1, gneiss), 1.5 m My^{-1} (CSB-2, gneiss) and 20.8 m My^{-1} (CSB-3, graywacke and mica schist). CSB-1 was collected from a ~1 m^2 outcrop of moderately weathered bedrock along the steep escarpment. CSB-2 was collected from a less weathered flat planar outcrop, ~150 m^2 just over the crest of the escarpment within the Blue Ridge province. CSB-3 was collected from a moderately weathered ~1 m^2 outcrop just over the crest of the escarpment within the Blue Ridge province.

Discussion

Cosmogenically determined erosion rates for basins draining the Blue Ridge escarpment indicate that it and the surrounding landscape are eroding slowly over a 10^4–10^5 year timescale (5.4–49 m My^{-1}). These basin scale rates are consistent with those estimated using ^{10}Be elsewhere in the southern and central Appalachian Mountains including samples from the Great Smoky Mountains, Shenandoah National Park, the

southeastern North American piedmont, and the New River basin (Duxbury et al., 2015; Granger et al., 1997; Matmon et al., 2003; Reusser et al., 2015). Similar to other Appalachian studies cited above, we find no correlation between basin area and erosion rate suggesting a lack of significant sediment storage (and thus post-hillslope cosmic-ray dosing) in the relatively small basins we sampled (Figure 4).

The three bedrock erosion rates we measured on the Blue Ridge escarpment are much more variable (1.5–106 m My^{-1}) than basin-averaged erosion rates, as would be expected from the lack of natural amalgamation. Bedrock erosion rates are generally consistent with, but both higher and lower than, those measured elsewhere in the Appalachians (4–11.5 m My^{-1} in the Georgia Piedmont, 2–9.5 m My^{-1} at Dolly Sods, West Virginia, 5–48 m My^{-1} in the Great Smoky Mountains, 2–11 m My^{-1} in the Shenandoah region, and 2.8–66 m My^{-1} in the Potomac and Susquehanna drainages as reported in Bierman et al., 1995; Hancock and Kirwan, 2007; Matmon et al., 2003; Portenga et al., 2013; Duxbury et al., 2015).

The cosmogenic data indicating slow rates of denudation integrated over 10^4–10^5 years near the Blue Ridge escarpment are consistent with existing thermochronologic data integrating over much longer (10^7–10^8 y) time scales. Spotila et al. (2003) used apatite (U-Th)/He thermochronology to calculate long-term (10^8 years) denudation rates of 8–22 m My^{-1} across the escarpment from the Blue Ridge toward the inner Piedmont. Spotila et al. (2003) also reported erosion rates across the escarpment calculated using

apatite fission track analysis in rock of 22–29 m My^{-1} integrated over a similar 10^8 year time scale. Similarly slow rates of denudation were reported for the southern Appalachians by McKeon et al. (2011) using apatite (U-Th)/He thermochronology.

Despite uncertainties in both the cosmogenic and thermochronologic methods, erosion rates, generated both cosmogenically and thermochronologically, fall within the same range. This similarity of slow erosion rates integrated over very different time scales is consistent with long-term stability of the landscape on and near the escarpment but must mask changes in erosion rates that occurred on intermediate time frames as suggested by the offshore record (Pazzaglia and Brandon, 1996) and geologic evidence of episodic drainage capture and the resulting incision and hillslope response (Prince et al., 2010, 2011; Prince and Spotila, 2013; Naeser et al., 2016). Interestingly, if the slope/erosion rate relationship we measured holds farther away from the escarpment, then the lower slopes of the outer Piedmont would suggest even lower erosion rates there – a suggestion verified by the data of Reusser et al. (2015). The deeper erosion of the inner Piedmont hypothesized by Spotila et al. (2003) is consistent with our new cosmogenic measurements.

The meaning of our data in the context of dynamic topography (Rowley et al., 2011) and subsequent landscape response (cf., Gallen et al., 2013 and Miller et al., 2013) is uncertain. Unlike Reuter (2005), we did not sample basins above and below knickzones and we did not specifically select basins for analysis (see supplementary data

figures for slope maps showing sample basins) because they did or did not have residual, flat-lying, undisected upland topography noted by Miller et al. (2013) and Prince and Spotila (2013). However, the significant relationship between average basin slope and ^{10}Be-derived erosion rate is consistent with either uplift of the landscape or incision due to stream capture over the last several million years if one accepts the hypothesis of Riebe et al. (2000) that slope and erosion rate are correlated only if there is effective base-level fall. Such an assertion is supported by Miller et al.'s (2013) more recent analysis of streams in the Susquehanna River basin.

Inferring sediment weathering and delivery processes

Grain-size specific ^{10}Be data from the Blue Ridge escarpment study area clearly indicate that clast transport processes and exposure histories are different than in the Great Smoky Mountains (Matmon et al., 2003). Rather than large grains having less ^{10}Be than smaller grains, in the four samples reported here (CS-01, CS-02, CS-03 and CS-06), the largest grains contain the most ^{10}Be suggesting that larger clasts have longer near-surface residence times than sand, perhaps because surface processes are unable to move larger clasts downslope efficiently. The existence of quartz veins in the micaceous schist and gneiss underlying the escarpment provide large, resistant quartz pebbles, the durability of which appears to at least in part contribute to the relationship between grain size and ^{10}Be concentration.

Inferring large-scale geomorphic process controls

Examining the Blue Ridge escarpment data set in the context of landscape-scale descriptors such as slope, allows us to infer geomorphic processes at the basin scale. For example, basin average slope and basin average erosion rate are clearly and positively related in the data set as a whole (Figure 3). A similar slope-erosion rate relationship has been found in the Great Smoky Mountains and in the Susquehanna Basin (Matmon et al., 2003; Reuter, 2005). A relationship between slope and erosion is inconsistent with an Appalachian landscape that is currently in dynamic equilibrium (non-directional, random change) as suggested by Hack (1960), who argued that slopes are adjusted to rock strength and thus eroding at the same rate throughout the landscape. It would appear that the processes that affect erosion and sediment transport on slopes, including soil creep, landsliding, and stream incision, are more efficient on steeper slopes (Heimsath et al., 1997; Montgomery and Brandon, 2002) than gentle slopes, and therefore the topography is not adjusted to rock strength as suggested by Hack – that is, erosion rates are not everywhere the same. This supports recent assertions by numerous authors that at least some parts of the Appalachians have been perturbed by uplift, drainage capture, and/or climate driven changes in erosion (e.g., Miller et al., 2013; Gallen et al., 2013; Prince and Spotila, 2013; Naeser et al., 2016).

Implications for the development of passive margin escarpments over time

In the areas we sampled, which are away from places where drainage capture events have been identified, the steep Blue Ridge escarpment is eroding more rapidly than the adjacent but more gently-sloped uplands and lowlands, thus providing a means for escarpment retreat over time. Since base level for the escarpment is set by the Piedmont, and since we estimate overall Piedmont lowering at 9.9 m My^{-1} and escarpment erosion at 20.5 m My^{-1} (Table 3) the difference suggests that while escarpment drainage basins are eroding slowly, they are eroding more rapidly than the Piedmont. We cannot reliably partition the erosion rate we estimate for the escarpment into vertical and horizontal components but if we assume that all the erosion is horizontal retreat (c.f., Vanacker et al., 2007) then the escarpment is retreating at most, about 20 m My^{-1} on average over the integration time of ^{10}Be at the erosion rates we measure (10^4–10^5 years).

Taken at face value, the cosmogenic data we collected (when extrapolated to much longer timeframes) do not support the hypothesis that the escarpment resulted from differential vertical erosion because the Piedmont is eroding on average more slowly than the Blue Ridge. The difference in modeled rates of lowering for the Piedmont (9.9 m My^{-1}) and Blue Ridge provinces (18.0 m My^{-1}) suggests that over time, relief across the escarpment should slowly decrease (~8 m My^{-1}) if the slope distributions and the erosion/slope relationship remain similar. Thus, we suggest, on the basis of our

measurements and modeling, that the Blue Ridge escarpment is both retreating (escarpment basin erosion) and lowering (differential erosion between the upland and the piedmont), albeit slowly.

On the basis of our data, if we extrapolate the maximum possible escarpment retreat rate assuming all erosion is retreat (~20 m My^{-1}), total escarpment retreat would be at most ~4 km since the opening of the Atlantic Ocean basin ~200 Ma. Existing geologic maps do not show normal faults closer than the Dan River-Danville rift boundary fault, ~35 km east of the escarpment base, so our calculation assumes the original position of the escarpment was at or near this rift basin. Whether the Dan River-Danville border fault is the actual margin that generated the Blue Ridge escarpment is unclear because the fault covers only ~25% of the length of the escarpment (Figure 1).

The cosmogenic erosion rate data suggest that the Blue Ridge escarpment is today eroding more than an order of magnitude more slowly than the mean rate of retreat that would be required to bring the landform steadily inland from the western boundary fault of the Dan River-Danville rift basin since the opening of the Atlantic Ocean. However, large drainage capture events, such as those postulated by Prince et al. (2010) and Naeser et al. (2001, 2016) would cause abrupt base-level fall and thus rapid landscape response as rivers incised into and beyond the escarpment speeding the average rate of escarpment retreat. Our data, because they come from stable parts of the landscape and because these capture events are episodic, are not capable of explicitly testing the process models of

Prince et al. (2010, 2011) and Prince and Spotila (2013). Sampling elsewhere along the escarpment could better test these process models.

Due to issues of both spatial and temporal scaling, it is challenging to consider both the cosmogenic nuclide and the extant thermochronologic data in the context of recent advances in the understanding of Appalachian topography. The existence of a thick crustal root below high Appalachian topography (Pratt et al., 1988; Wagner et al., 2012) and the idea of recent rejuvenation of such topography by surface response to mantle dynamics (Rowley et al., 2013) both provide the driving force for steep slopes that are correlated in our study with higher measured rates of basin-scale erosion. These solid Earth processes which can drive land surface change may or may not be related to the observations of Prince et al. (2010, 2011) and Prince and Spotila (2013) concerning drainage capture events which would themselves increase local stream and hillslope gradients and thus local erosion rates (Miller et al., 2013). Better dating of both solid Earth changes (dynamic topographic response) and surface Earth responses, such as drainage capture, combined with sampling campaigns directly targeted at basins shown to be in disequilibrium (c.f., Miller et al., 2013) will better inform our understanding of what appears to be the long-lasting yet dynamic surface topography of the southern Appalachian Mountains.

Conclusions

Cosmogenic isotopic data collected from four transects along the Blue Ridge escarpment indicate that it and the bordering Blue Ridge highlands and Piedmont lowlands are eroding slowly (5.4–49 m My^{-1} for fluvial sediment and 1.5–106 m My^{-1} for bedrock). The positive relationship between average basin slope and basin-scale erosion rates is consistent with a non-equilibrium landscape in the sense of Riebe et al. (2000) thus providing evidence for base-level change. Calculated rates of Blue Ridge escarpment retreat, based on our data collected from areas of the escarpment unaffected by recent drainage capture, are too slow to support a model of long-term landscape evolution in which the escarpment steadily retreated from the closest potential rift margin boundary fault. Evidence collected by others in areas we did not sample suggests that periodic drainage captures may result in episodes of more rapid escarpment retreat that we document isotopically. Targeted sampling in areas where recent incision has occurred would test the importance of such captures for the evolution of Blue Ridge Escarpment landscapes.

Acknowledgements

This research was supported by the National Science Foundation grant EAR-0310208. We thank C. Coutu for field assistance and D. Rizzo for statistical consulting. J. Roering, A. Matmon, and un-named individuals improved the paper with critical reviews.

References Cited

Baldwin JA, Whipple KX, and Tucker GE. 2003. Implications of the shear stress river incision model for the timescale of postorogenic decay of topography: *Journal of Geophysical Research* **108**: 2158. DOI: 10.1029/2001JB000550.

Balco G, Stone JO, Lifton NA, Dunai TJ. 2008. A complete and easily accessible means of calculating surface exposure ages or erosion rates from ^{10}Be and ^{26}Al measurements: *Quaternary Geochronology* **3**: 174-195. DOI: 10.1016/j.quageo.2007.12.001.

Bank GC. 2002. Testing the origins of the Blue Ridge escarpment (Masters thesis): Blacksburg, Virginia Tech, 119 p.

Barron EJ. 1989. Climate variations and the Appalachians from the Late Paleozoic to the present: results from model simulations: *Geomorphology* **2**: 99-118. DOI: 10.1016/0169-555X(89)90008-1.

Battiau-Queney Y. 1989. Constraints from deep crustal structure on long-term landform development of the British Isles and eastern United States: *Geomorphology* **2**: 53-70. DOI: 10.1016/0169-555X(89)90006-8.

Bierman PR, Caffee MW. 2002. Cosmogenic exposure and erosion history of ancient Australian bedrock landforms: *Geological Society of America Bulletin* **114**: 787-803. DOI: 10.1130/0016-7606(2002)114<0787:CEAEHO>2.0.CO;2.

Bierman PR, Caffee MW. 2001. Slow rates of rock surface erosion and sediment production across the Namib Desert and escarpment, Southern Africa: *American Journal of Science* **301**: 326-358. DOI: 10.2475/ajs.301.4-5.326.

Bierman PR, Steig EJ. 1996. Estimating rates of denudation and sediment transport using cosmogenic isotope abundances in sediment: *Earth Surface Processes and Landforms* **21**: 125-139.

Brown ET, Stallard RF, Larsen MC, Bourles DL, Raisbeck GM, Yiou F. 1998. Determination of predevelopment denudation rates of an agricultural watershed (Cayaguas River, Puerto Rico) using in-situ-produced ^{10}Be in river-borne quartz: *Earth and Planetary Science Letters* **160**: 723-728. DOI: 10.1016/S0012-821X(98)00123-X.

Brown RW, Gallagher K, Gleadow AJW, Summerfield MA. 2000. Morphotectonic evolution of the South Atlantic margins of Africa and South America, *in* Summerfield, MA, ed., Geomorphology and Global Tectonics: Chichester, Wiley: 255-281.

Child D, Elliott G, Mifsud C, Smith AM, Fink D. 2000. Sample processing for earth science studies at ANTARES: *Nuclear Instruments and Methods in Physics Research B Beam Interactions with Materials and Atoms* **172**: 856–860. DOI: 10.1016/S0168-583X(00)00198-1.

Chu R, Leng W, Helmberger DV, Gurnis M. 2013. Hidden hotspot track beneath the eastern United States: *Nature Geoscience* **6**: 963–966. DOI: 10.1038/ngeo1949.

Cockburn HAP, Brown RW, Summerfield MA, Seidl MA. 2000. Quantifying passive margin denudation and landscape development using a combined fission-track thermochronology and cosmogenic isotope analysis approach: *Earth and Planetary Science Letters* **179**: 429-435. DOI: 10.1016/S0012-821X(00)00144-8.

Cockburn HAP, Seidl MA, Summerfield MA. 1999. Quantifying denudation rates on inselbergs in the central Namib Desert using in situ-produced cosmogenic ^{10}Be and ^{26}Al: *Geology* **27**: 399-402. DOI: 10.1130/0091-7613(1999)027<0399:QDROII>2.3.CO;2.

Davis WM. 1899. The geographical cycle: Geographical Journal **14**: 481-504. DOI: 10.2307/1774538.

— 1903. The stream contest along the Blue Ridge. *Geol. Soc: Philadelphia Bull* **3**: 213-244.

Delcourt PA, Delcourt HR. 1984. Late Quaternary paleoclimates and biotic responses in eastern North America and the western North Atlantic Ocean: *Paleogeography, Paleoclimatology, Paleoecology* **48**: 263-284. DOI: 10.1016/0031-0182(84)90048-8.

Dietrich RV. 1957. Origin of the Blue Ridge Escarpment directly southwest of Roanoke, Virginia: *Virginia Journal of Science* **9**: 233-246.

— 1959. Geology and mineral resources of Floyd County of the Blue Ridge Upland, southwestern Virginia: Bulletin of the Virginia Polytechnic Institute no. 134 160 p.

Duxbury J, Bierman PR, Portenga EW, Pavich MJ, Southworth S, Freeman, SPHT. 2015. Erosion rates in and around Shenandoah National Park, Virginia, determined using analysis of cosmogenic ^{10}Be: *American Journal of Science* **315**: 46-76. DOI: 10.2475/01.2015.02.

Fleming A, Summerfield MA, Stone JO, Fifield LK, Cresswell RG. 1999. Denudation rates for the southern Drakensberg Escarpment, SE Africa, derived from in-situ-produced cosmogenic ^{36}Cl; initial results: *Journal of the Geological Society of London* **156**: 209-212. DOI: 10.1144/gsjgs.156.2.0209.

Gallen SF, Wegmann KW, Bohnenstiehl DR. 2013. Miocene rejuvenation of topographic relief in the southern Appalachians: *GSA Today*: **23** 4-10.

Gilchrist AR, Summerfield MA. 1990. Tectonic models of passive margin evolution and their implications for theories of long-term landscape development, *in* Kirkby MJ ed. Process Models and Theoretical Geomorphology: Wiley, Chichester: 55-84.

Granger DE, Kirchner JW, Finkel RC. 1997. Quaternary downcutting rate of the New River, Virginia, measured from differential decay of cosmogenic ^{26}Al and ^{10}Be in cave-deposited alluvium: *Geology* **25**: 107-110. DOI: 10.1130/0091-7613(1997)025<0107:QDROTN>2.3.CO;2.

Hack JT. 1960. Interpretation of erosional topography in humid temperate regions: *American Journal of Science* **258A**: 80-97.

— 1975. Dynamic equilibrium and landscape evolution, *in* Melhorn WN, and Flemal RC, eds., Theories of landform development: Binghamton, N.Y., State University of New York at Binghamton: 87-102.

— 1982. Physiographic divisions and differential uplift in the Piedmont and Blue-Ridge: U.S. Geological Survey Professional Paper 1265 49 p.

Hancock GS, Kirwan ML. 2007. Summit erosion rates deduced from ^{10}Be: Implications for relief production in the central Appalachians: *Geology* **35**: 89-92. DOI: 10.1130/G23147A.1.

Hayes CW, Campbell MR. 1894. Geomorphology of the Southern Appalachians Published by the National Geographic Society.

Heimsath AM, Chappell J, Finkel RC, Fifield K, Alimanovic A. 2006. Escarpment erosion and landscape evolution in southeastern Australia: *Geological Society Of America Special Paper* **398**: 173-190. DOI: 10.1130/2006.2398(10).

Heimsath AM, Dietrich WE, Nishiizumi K, Finkel RC. 1997. The soil production function and landscape equilibrium: *Nature* **388**: 358-361.

Hewawasam T, von Blackenburg F, Schaller M, Kubik P. 2003. Increase of human over natural erosion rates in tropical highlands constrained by cosmogenic nuclides: *Geology* **31**: 597-600. DOI: 10.1130/0091-7613(2003)031<0597:IOHONE>2.0.CO;2.

Japsen, P, Chalmers JA, Green PF, Bonow JM. 2012. Elevated, passive continental margins: Not rift shoulders, but expressions of episodic, post-rift burial and

exhumation: *Global and Planetary Change* **90-91**: 73–86. DOI: 10.1016/j.gloplacha.2011.05.004.

Judson S. 1975. Evolution of the Appalachian topography: Theories of landform development, Publications in Geomorphology: New York, State University of New York at Binghamton: 29–44.

Jungers MC, Bierman PR, Matmon A, Nichols KK, Larsen J, Finkel R. 2009. Tracing hillslope sediment production and transport with in situ and meteoric ^{10}Be: *Journal of Geophysical Research – Earth Surface*: **114** (F04020).

Kirchner JW, Finkel RC, Riebe CS, Granger DE, Clayton JL, King JG, Megahan WF. 2001. Mountain erosion over 10 yr, 10 k.y., and 10 m.y. time scales: *Geology* **29**: 591-594. DOI: 10.1130/0091-7613(2001)029<0591:MEOYKY>2.0.CO;2.

Kohl CP, Nishiizumi K. 1992. Chemical isolation of quartz for measurement of *in-situ* -produced cosmogenic nuclides: *Geochimica et Cosmochimica Acta* **56**: 3583-3587. DOI: 10.1016/0016-7037(92)90401-4.

— 1991 Cosmic ray labeling of erosion surfaces; in situ nuclide production rates and erosion models: *Earth and Planetary Science Letters* **104**: 424-439. DOI: 10.1016/0012-821X(91)90220-C.

Mandal SK, Lupker M, Burg J-P, Valla PG, Haghipour N, Christl M. 2015. Spatial variability of ^{10}Be-derived erosion rates across the southern Peninsular Indian

escarpment: A key to landscape evolution across passive margins: *Earth and Planetary Science Letters* **425**: 154–167. DOI: 10.1016/j.epsl.2015.05.050.

Matmon A, Bierman PR, Enzel Y. 2002. Pattern and tempo of great escarpment erosion: *Geology* **30**: 1135-1138. DOI: 10.1130/0091-7613(2002)030<1135:PATOGE>2.0.CO;2.

Matmon A, Bierman PR, Larsen J, Southworth CS, Pavich MJ, Finkel RC, and Caffee MW. 2003. Erosion of an ancient mountain range, the Great Smoky Mountains, North Carolina and Tennessee: *American Journal of Science* **303**: 817-855. DOI: 10.2475/ajs.303.9.817.

Matmon, A, Mushkin A, Enzel Y, Grodek, T. 2013. Erosion of a granite inselberg, Gross Spitzkoppe, Namib Desert: *Geomorphology* **201**: 52-59. DOI: 10.1016/j.geomorph.2013.06.005.

Matsuoka, N and Murton, J. 2008. Frost weathering: recent advances and future directions: *Permafrost and Periglacial Processes* **19**: 1099-1530. DOI: 10.1002/ppp.620.

McKeon RE, Zeitler PK, Pazzaglia FJ, Idleman BD, Enkelmann E. 2011. Decay of an old orogen; inferences about Appalachian landscape evolution from low-temperature thermochronology: *Geological Society of America Bulletin*: **126**: 31-46.

Montgomery DR, Brandon MT. 2002. Topographic controls on erosion rates in tectonically active mountain ranges: *Earth and Planetary Science Letters* **201**: 481-489. DOI: 10.1016/S0012-821X(02)00725-2.

Miller SR, Sak PB, Kirby E, Bierman PR. 2013. Neogene rejuvenation of central Appalachian topography: Evidence for differential rock uplift from stream profiles and erosion rates: *Earth and Planetary Science Letters* **369-370**: 1-12. DOI: 10.1016/j.epsl.2013.04.007.

Naeser CW, Naeser ND, Kunk MJ, Morgan BAI, Schultz AP, Southworth CS, and Weems RE. 2001. Paleozoic through Cenozoic uplift, erosion, stream capture, and deposition history in the Valley and Ridge, Blue Ridge, Piedmont, and Coastal Plain Provinces of Tennessee, North Carolina, Virginia, Maryland, and District of Columbia: *Geological Society of America Abstracts with Programs* **133**.

Naeser CW, Naeser ND, Newell, WL, Southworth CS, Edwards, LE and Weems RE. 2016. Erosional and depositional history of the Atlantic passive margin as recorded in detrital zircon fission-track ages and lithic detritus in Atlantic Coastal plain sediments: *American Journal of Science February* **316**:110-168. doi:10.2475/02.2016.02

Nishiizumi K, Imamura M, Caffee MW, Southon JR, Finkel RC, McAninch J. 2007. Absolute calibration of ^{10}Be AMS standards: *Nuclear Inst. and Methods in Physics Research B* **258**: 403-413. DOI: 10.1016/j.nimb.2007.01.297.

Ollier CD. 1984. Morphotectonics of continental margins with great escarpments, *in* Morisawa, M, and Hack, JT, ed., Tectonic Geomorphology, Volume International Series 15: Binghamton Symposia in Geomorphology: Boston, Unwin Hayman: 3-25.

Pazzaglia FJ, Brandon MT. 1996. Macrogeomorphic evolution of the post-Triassic Appalachian Mountains determined by deconvolution of the offshore basin sedimentary record: *Basin Research* **8**: 255-278.

Pazzaglia FJ, Gardner TW. 1994. Late Cenozoic flexural deformation of the middle U. S. Atlantic passive margin: *Journal of Geophysical Research B Solid Earth and Planets* **99**: 12,143-12,157. DOI: 10.1029/93JB03130.

Persano C, Stuart FM, Bishop P, Barfod DN. 2002. Apatite (U-Th)/He age constraints on the development of the Great Escarpment on the southeastern Australian passive margin: *Earth and Planetary Science Letters* **200**: 79-90. DOI: 10.1016/S0012-821X(02)00614-3.

Portenga EW, Bierman PR. 2011. Understanding Earth's eroding surface with ^{10}Be: *GSA Today* **21**: 4-10. DOI: 10.1130/G111A.1.

Portenga EW, Bierman PR, Rizzo DM, Rood DH. 2013. Low rates of bedrock outcrop erosion in the central Appalachian Mountains inferred from in situ ^{10}Be: *Geological Society of America Bulletin* **125**: 201-215. DOI: 10.1130/B30559.1.

Pratt TL, Çoruh C, Costain JK, Glover L. 1988. A geophysical study of the Earth's crust in central Virginia: Implications for Appalachian crustal structure. *Journal of Geophysical Research* **93**: 6649–6667. DOI: 10.1029/JB093iB06p06649.

Prince PS, Spotila JA, Henika WS. 2011. Stream capture as driver of transient landscape evolution in a tectonically quiescent setting: *Geology* **39**: 823-826. DOI: 10.1130/G32008.1.

Prince PS, Spotila JA, Henika WS. 2010. New physical evidence of the role of stream capture in active retreat of the Blue Ridge escarpment, southern Appalachians: *Geomorphology* **123**: 305-319. DOI: 10.1016/j.geomorph.2010.07.023.

Prince, PS, Spotila, J A. 2013. Evidence of transient topographic disequilibrium in a landward passive margin river system: knickpoints and paleo-landscapes of the New River basin, southern Appalachians: *Earth Surface Processes and Landforms* **38**: 1685-1699. DOI: 10.1002/esp.3406.

Reusser L, Bierman PR, Rood D. 2015. Quantifying human impacts on rates of erosion and sediment transport at a landscape scale: *Geology* **43**: 171-174. DOI: 10.1130/G36272.1.

Reuter JM. 2005. Erosion Rates and Patterns Inferred from Cosmogenic ^{10}Be in the Susquehanna River Basin. M.S. : University of Vermont, 172 p.

Richmond GM, Fullerton DS. 1986. Introduction To Quaternary Glaciations in the United States of America, *in* Sibrava, V, Bowen, DQ, and Richmond, GM, eds.,

Quaternary Glaciations in the Northern Hemisphere: Oxford, New York, Pergamon Press: 3-10.

Riebe CS, Kirchner JW, Granger DE, Finkel RC. 2000. Erosional equilibrium and disequilibrium in the Sierra Nevada, inferred from cosmogenic ^{26}Al and ^{10}Be in alluvial sediment: *Geology* **28**: 803-806. DOI: 10.1130/0091-7613(2000)28<803:EEADIT>2.0.CO;2.

Roper PJ, Justus PS. 1973. Polytectonic evolution of the Brevard zone: *American Journal of Science* **273A**: 105-132.

Rowley DB, Forte AM, Moucha R, Mitrovica JX, Simmons NA, Grand, SP. 2013. Dynamic topography change of the eastern United States since 3 million years ago: *Science* **340**: 1560-1563. DOI: 10.1126/science.1229180.

Salgado AAR, Marent BR, Cherem LFS, Bourlès D, Santos LJC, Braucher R, Barreto HN. 2013. Denudation and retreat of the Serra do Mar escarpment in southern Brazil derived from *in situ*-produced ^{10}Be concentration in river sediment: *Earth Surface Processes and Landforms* **39**: 311–319. DOI: 10.1002/esp.3448.

Scharf TE, Codilean AT, de Wit M, Jansen JD, Kubik PW. 2013. Strong rocks sustain ancient postorogenic topography in southern Africa: *Geology* **41**: 331–334. DOI: 10.1130/G33806.1.

Schlische RW. 1993. Anatomy and evolution of the Triassic-Jurassic continental rift system, eastern North America: *Tectonics* **12**: 1026-1042. DOI: 10.1029/93TC01062.

Schmandt B, Lin FC. 2014. P and S wave tomography of the mantle beneath the United States: *Geophysical Research Letters* **41**: 6342-6349. DOI: 10.1002/2014GL061231.

Seidl MA, Weissel JK, Pratson LF. 1996. The kinematics and pattern of escarpment retreat across the rifted continental margin of SE Australia: *Basin Research* **8**: 301-316.

Slingerland RL, Furlong KP. 1989. Geodynamic and Geomorphic Evolution of the Permo-Triassic Appalachian Mountains: *Geomorphology* **2**: 23-27. DOI: 10.1016/0169-555X(89)90004-4.

Spotila JA, Bank GC, Reiners PW, Naeser CW, Naeser ND, Henika WS. 2004. Origin of the Blue Ridge escarpment along the passive margin of Eastern North America: *Basin Research* **16**: 41-63. DOI: 10.1111/j.1365-2117.2003.00219.x.

Summerfield MA, Brown RW, Van Der Beek P, Braun J. 1997. Drainage divides, denudation, and the morphotectonic evolution of high-elevation passive margins: *Geological Society of America Abstracts with Programs* **29**: 476.

Tucker GE, Slingerland RL. 1994. Erosional dynamics, flexural isostasy, and long-lived escarpments: A numerical modeling study: *Journal of Geophysical Research* **99**: 12,229-12,243. DOI: 10.1029/94JB00320

Vanacker V., von Blackenburg F., Hewawasam T., and Kubik PW. 2007. Constraining landscape development of the Sri Lankan escarpment with cosmogenic nuclides in river sediment: *Earth and Planetary Science Letters* **253**: 402-414. DOI: 10.1016/j.epsl.2006.11.003.

Wagner L S, Metcalf K, Stewart K. 2012. Crustal-scale shortening structures beneath the Blue Ridge Mountains, North Carolina, USA: *Lithosphere* **4**: 242-256. DOI: 10.1130/L184.1.

White WA. 1950. Blue Ridge front; a fault scarp: *Bulletin of the Geological Society of America* **61**: 1309. DOI: 10.1130/0016-7606(1950)61[1309:BRFFS]2.0.CO;2.

Witt AC, Smith MS, Latham RS, Douglas TJ, Gillon KA, Fuemmeler SJ, Bauer JB, Wooten RM. 2007. Life, death, and landslides: the August 13-14 1940 storm event in Watauga County, North Carolina: 2007 *Southeastern Section Meeting, Geological Society of America Abstracts with Programs* **39**: 76.

Xu, S, Freeman SPHT, Rood DH, Shanks RM. 2015. Decadal ^{10}Be, ^{26}Al and ^{36}Cl QA measurements on the SUERC accelerator mass spectrometer: *Nuclear Instruments and Methods B: Beam Interactions with Materials and Atoms* **361**: 39–42. DOI: 10.1016/j.nimb.2015.03.064.

Figure Captions

Figure 1 – Main shaded relief map shows the Atlantic margin of the United States and the extent of the Blue Ridge and Piedmont physiographic provinces, the location of the Blue Ridge escarpment zone (gray), the location of the Brevard fault zone (dashed line), and the location of the Dan River-Danville basin (solid black) – the western-most Mesozoic rift basin. Upper inset cross section indicates the asymmetry of the drainage divide at the top of the Blue Ridge escarpment (cross section modified from Spotila et al., 2004). Thin gray lines are state borders. Black boxes in the main figure, labeled A, B, C, and D refer to the respective panels below, which show sample collection locations and the upstream area from which collected sediment is contributed. Gray shaded areas demarcate the Escarpment Zone (EZ), the transition between the Blue Ridge (BR) and Piedmont (P) provinces. Circles represent sediment samples and black triangles represent outcrop samples. White lines in each panel are generally normal to the escarpment. Shaded relief base maps are the World Shaded Relief map, produced and made available by ESRI.

Figure 2 – Landscape photographs of each province and large scale province location map showing Blue Ridge (BR), Escarpment, and Piedmont (P): A) Blue Ridge near sample site CS-27 showing subdued relief. B) View of escarpment near Fancy Gap, VA showing heavy vegetation and steep topography. C) Piedmont

view facing east from the escarpment near Chimney Rock, NC showing subdued relief and stream network flowing toward the coast.

Figure 3 – Erosion rates are positively correlated to mean basin slope for each province and for the entire sample population. Inset shows average basin erosion rate (^{10}Be) and average basin slope (sampled basins only) for each physiographic province are well and positively correlated. Uncertainties are plotted as one standard error of the mean.

Figure 4 – No relationship exists between measured erosion rates and basin area.

Figure 5 – No relationship exists between measured erosion rates and mean basin elevation.

Figure 6 – Cumulative probability plot of average basin slope for each province showing how well our sampled basins match the entire population of basins for each of the three provinces. Each sampled basin is plotted as a symbol on the cumulative probability curve of all province basins as determined by GIS. Inset histograms show distribution of average basin slopes within each province: Blue Ridge, escarpment, Piedmont.

Figure 7 – No systematic relationship exists between measured ^{10}Be concentration and grain size fraction. Errors are propagated 1σ uncertainties in analytical measurements.

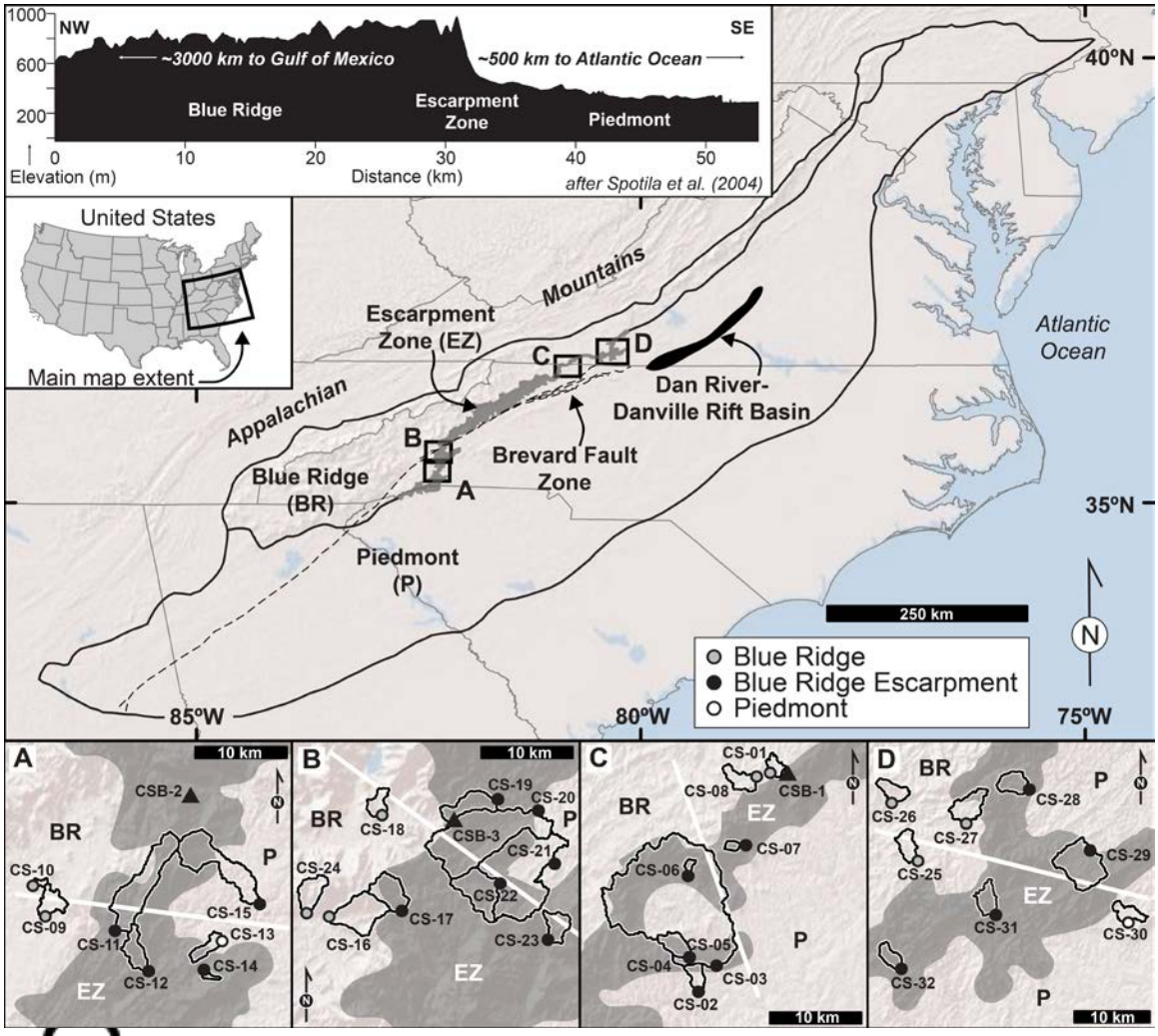

Figure 1

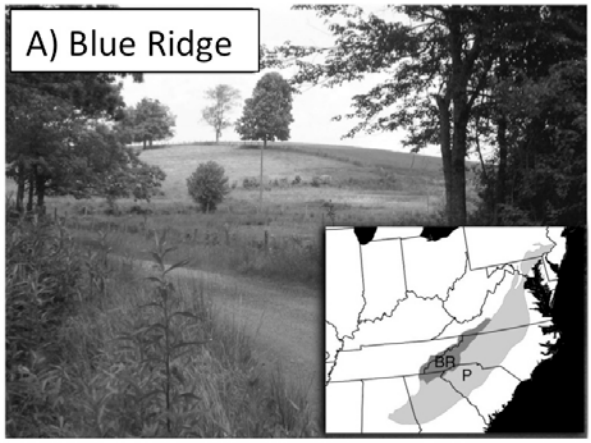

Figure 2

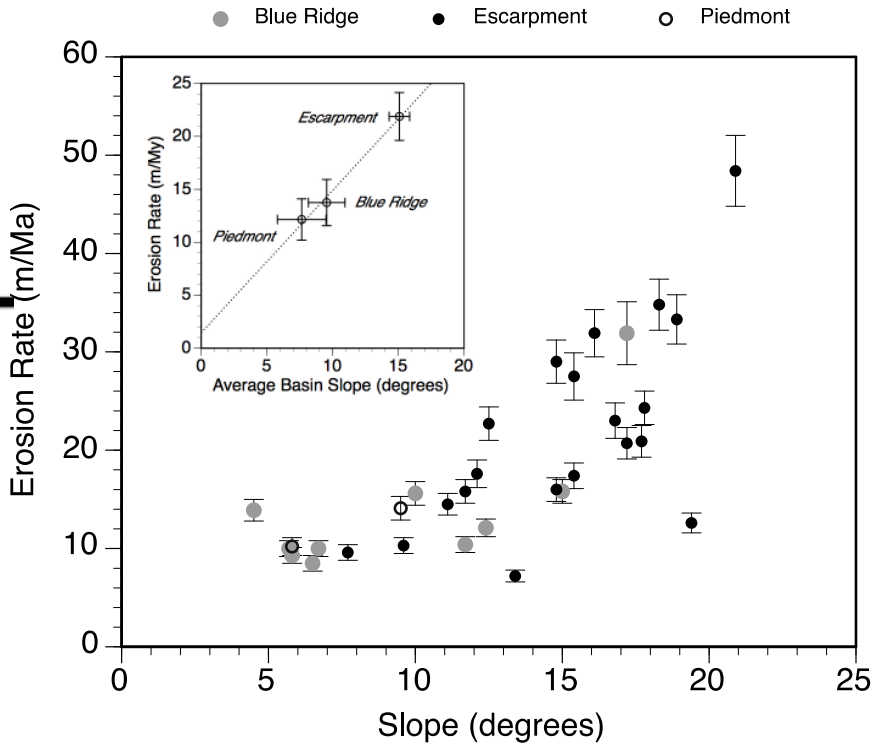

Figure 3

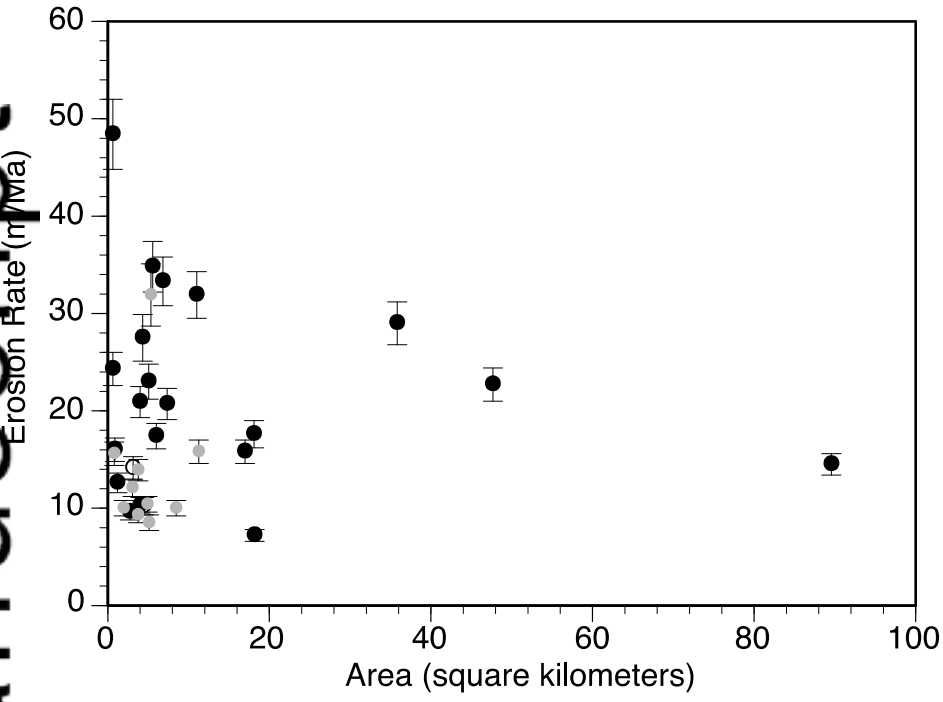

Figure 4

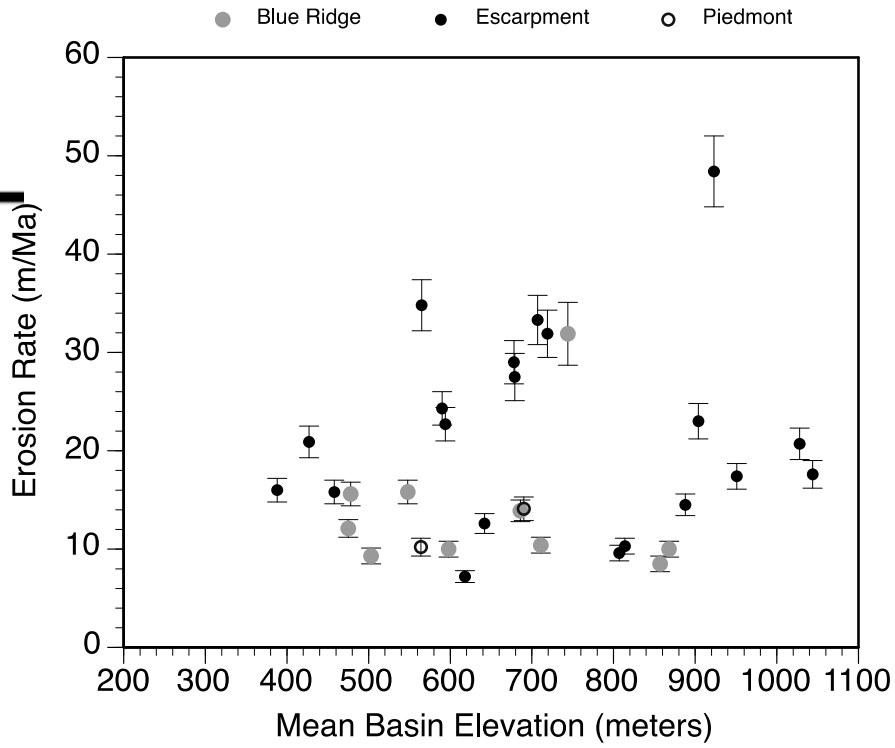

Figure 5

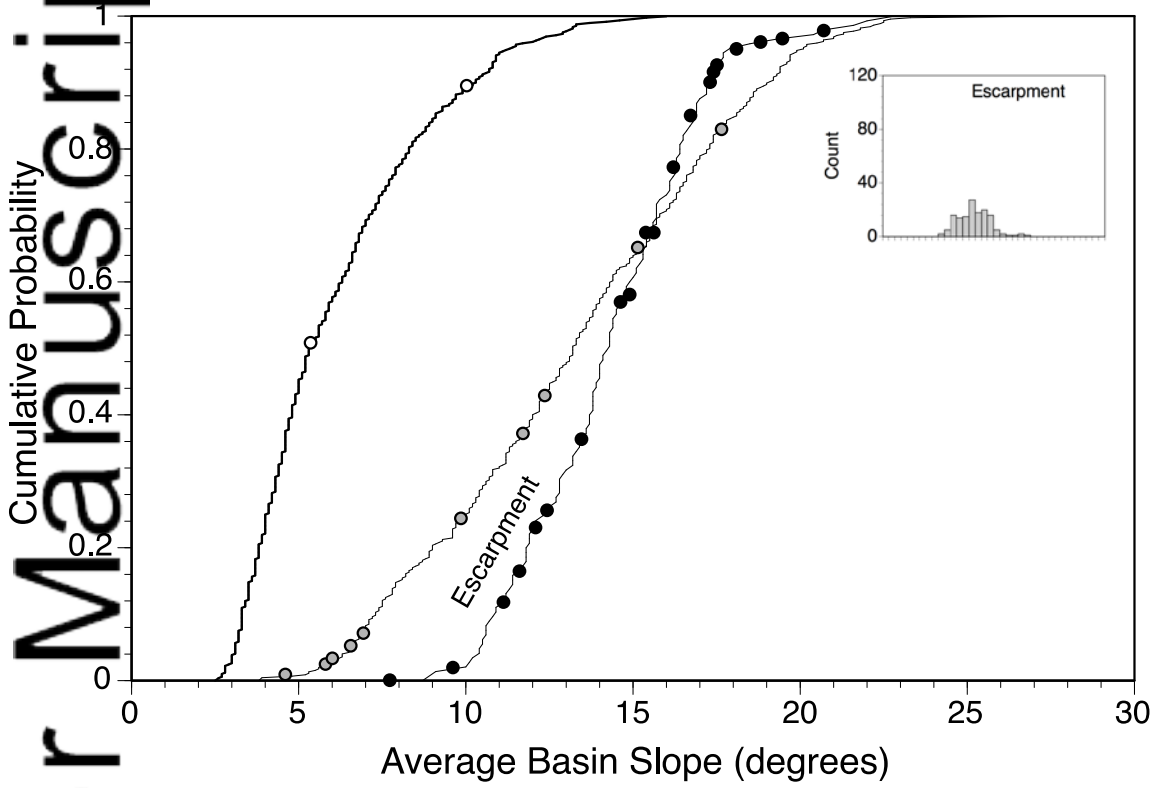

Figure 6

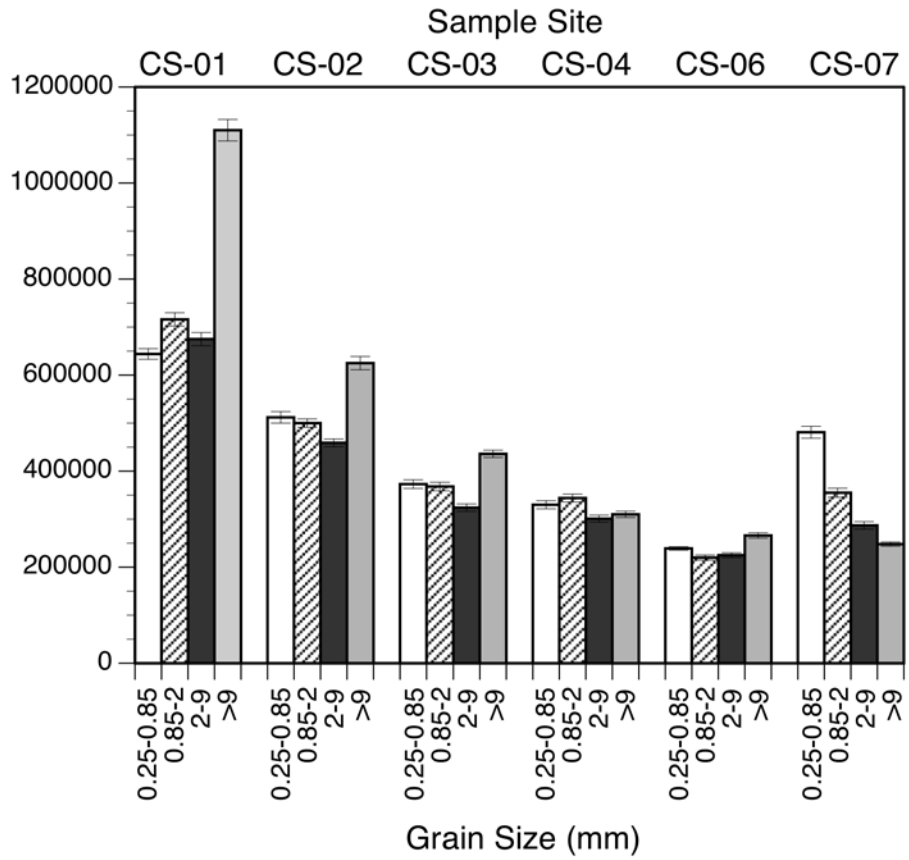

Figure 7

Table 1. Sample locations and basin characteristics

Sample ID	Latitude	Longitude	Area	%BRE	Province	Relief	Mean Slope (°)	Median Slope (°)	Mean Elevation	Effective Elevation

Table 2. Cosmogenic nuclide data and erosion rates

Sample ID	Grain Size (mm)	^{9}Be Carrier (µg)	Quartz (g)	AMS ID#	Blank corrected ^{10}Be/^{9}Be ($\times 10^{-13}$)	Measured ^{10}Be (atoms/g)	Erosion rate (m My^{-1})
CS-01	0.25-0.85	304	37.13	BE22565	11.80 ± 0.20	644000 ± 11100	10.0 ± 0.8
CS-01	0.85-2	305	39.27	BE22566	13.80 ± 0.27	716000 ± 13900	
CS-01	2-9	304	40.09	BE22567	13.30 ± 0.27	675000 ± 13700	
CS-01	>9	303	35.36	BE22568	19.50 ± 0.39	1110000 ± 22400	
CS-02	0.25-0.85	300	40.93	BE22581	10.50 ± 0.25	512000 ± 12000	9.6 ± 0.8
CS-02	0.85-2	307	40.06	BE22582	9.77 ± 0.17	500000 ± 8700	
CS-02	2-9	299	40.02	BE22583	9.20 ± 0.16	459000 ± 8010	
CS-02	>9	306	39.40	BE22584	12.00 ± 0.27	625000 ± 13800	
CS-03	0.25-0.85	303	32.80	BE22569	6.04 ± 0.15	373000 ± 9010	14.5 ± 1.1
CS-03	0.85-2	304	37.83	BE22570	6.85 ± 0.17	368000 ± 8860	
CS-03	2-9	300	40.11	BE22571	6.49 ± 0.16	324000 ± 7770	
CS-03	>9	303	40.06	BE22585	8.62 ± 0.15	436000 ± 7620	
CS-04	0.25-0.85	252	22.44	BE22533	4.39 ± 0.11	330000 ± 8410	16.0 ± 1.2
CS-04	0.85-2	253	29.74	BE22534	6.07 ± 0.15	344000 ± 8290	
CS-04	2-9	252	31.27	BE22535	5.59 ± 0.14	301000 ± 7270	
CS-04	>9	252	33.61	BE22536	6.19 ± 0.13	310000 ± 6620	
CS-05	0.25-0.85	305	40.10	BE22586	9.45 ± 0.23	480000 ± 11800	10.3 ± 0.8
CS-06	0.25-0.85	251	40.69	BE22541	5.81 ± 0.09	239000 ± 3510	24.3 ± 1.7
CS-06	0.85-2	253	40.15	BE22542	5.22 ± 0.13	220000 ± 5400	
CS-06	2-9	253	24.84	BE22543	3.31 ± 0.07	225000 ± 5100	
CS-06	>9	253	20.61	BE22544	3.24 ± 0.07	266000 ± 5680	
CS-07	0.25-0.85	303	29.74	BE22549	7.06 ± 0.18	481000 ± 12400	12.6 ± 1.0
CS-07	0.85-2	301	24.17	BE22550	4.27 ± 0.11	355000 ± 9450	
CS-07	2-9	302	23.66	BE22551	3.37 ± 0.09	287000 ± 7810	
CS-07	>9	307	31.13	BE22552	3.76 ± 0.07	248000 ± 4400	
CS-08	0.25-0.85	314	24.47	BE22587	7.96 ± 0.19	682000 ± 16200	9.3 ± 0.8
CS-09	0.25-0.85	411	28.26	BE23185	4.28 ± 0.09	416000 ± 8670	13.9 ± 1.1
CS-10	0.25-0.85	408	26.98	BE23186	3.74 ± 0.08	378000 ± 8190	15.6 ± 1.2
CS-11	0.25-0.85	244	20.48	b2276	4.47 ± 0.10	356000 ± 8320	17.6 ± 1.4
CS-12	0.25-0.85	247	22.18	b2277	3.39 ± 0.11	252000 ± 8500	23.0 ± 1.8
CS-13	0.25-0.85	405	25.01	BE23187	3.13 ± 0.12	339000 ± 12500	14.1 ± 1.2
CS-14	0.25-0.85	304	34.74	BE23189	2.06 ± 0.06	121000 ± 3610	49.2 ± 3.6
CS-14 (rep)	0.25-0.86	245	24.34	b2278	1.84 ± 0.06	124000 ± 4000	47.6 ± 3.5
CS-15	0.25-0.85	303	34.67	BE23190	5.49 ± 0.11	321000 ± 6490	15.8 ± 1.2
CS-16	0.25-0.85	303	40.10	BE23191	8.37 ± 0.16	422000 ± 8070	15.8 ± 1.2
CS-17	0.25-0.85	248	10.57	b2279	2.27 ± 0.07	355617 ± 10500	20.7 ± 1.6
CS-18	0.25-0.85	304	31.82	BE23192	8.03 ± 0.15	513000 ± 9840	12.1 ± 0.9
CS-19	0.25-0.85	304	30.35	BE23193	2.81 ± 0.07	188000 ± 4960	33.3 ± 2.5
CS-20	0.25-0.85	303	26.45	BE23213	2.76 ± 0.09	211000 ± 6570	29.0 ± 2.2
CS-21	0.25-0.85	309	40.90	BE23194	4.96 ± 0.10	251000 ± 5160	22.7 ± 1.7
CS-22	0.25-0.85	304	29.06	BE23208	2.82 ± 0.08	197000 ± 5460	31.9 ± 2.4
CS-23	0.25-0.85	306	40.02	BE23195	4.32 ± 0.23	221000 ± 11800	27.5 ± 2.4
CS-24	0.25-0.85	303	25.00	BE23214	2.78 ± 0.07	226000 ± 5890	34.1 ± 2.6
CS-24 (rep)	0.25-0.86	247	22.64	b2280	3.51 ± 0.10	256000 ± 7010	29.6 ± 2.3
CS-25	0.25-0.85	307	35.91	BE23197	13.30 ± 0.50	761000 ± 28500	8.5 ± 0.8
CS-26	0.25-0.85	303	20.03	BE23215	6.36 ± 0.14	643000 ± 13900	10.4 ± 0.8
CS-27	0.25-0.85	306	32.03	BE23209	10.60 ± 0.30	680000 ± 19300	10.0 ± 0.8
CS-28	0.25-0.85	304	21.64	BE23210	3.53 ± 0.10	331000 ± 9210	17.4 ± 1.3
CS-29	0.25-0.85	301	38.42	BE23198	13.50 ± 0.26	704000 ± 13770	7.2 ± 0.6
CS-30	0.25-0.85	304	40.05	BE23199	9.53 ± 0.47	483000 ± 23700	9.9 ± 0.9
CS-30 (rep)	0.25-0.86	247	19.74	b2283	5.60 ± 0.29	459390 ± 24100	10.4 ± 1.0
CS-31	0.25-0.85	307	32.12	BE23200	2.84 ± 0.08	181000 ± 5330	34.8 ± 2.6
CS-32	0.25-0.85	306	34.91	BE23211	4.60 ± 0.11	269000 ± 6260	20.9 ± 1.6
CSB-1	NA	304	26.40	BE23201	0.89 ± 0.05	68800 ± 4030	106.3 ± 9.5
CSB-2	NA	303	13.08	BE23216	17.50 ± 0.35	2710000 ± 54800	1.5 ± 0.2
CSB-3	NA	303	28.71	BE23202	4.73 ± 0.17	334000 ± 11900	20.8 ± 1.7

1. Analytic uncertainty is one standard deviation. Samples run at Livermore National Laboratory (BE #) were normalized to KNSTD3110 with assumed ratio of 3150 x 10^{-15}. Samples run at SUERC (b#) were normalized to NIST standard with assumed ratio of 30600 x 10^{-15}

2. Measured ratios were corrected for process blanks run with each batch of samples and the uncertainty was propagated in quadrature. Process blanks (n=10) for samples prepared at the University of Vermont and analyzed at Livermore National Laboratory (BE#) averaged 2.1±0.3 x 10^{-14}. A single process blank for samples prepared and analyzed at SUERC (b #) returned a ratio of 1.1±0.1 x 10^{-14}. Blank corrections were applied specifically for samples measured on the different accelerators.

3. Erosion rates calculated using CRONUS (Balco et al., 2008); Wrapper script: 2.2, Main calculator: 2.1, Objective function: 2.0, Constants: 2.2.1, Muons: 1.1; global production rate and Lal/Stone scaling with no geomagnetic forcing. External uncertainty reported at one standard deviation.

Table 3. Summary of measured and modeled erosion rates

				eled basins				Regression slope		
Blue Ridge	9.6±4.4	10	13.3±4.3	447	13.7	14.1	18.0	1.132	2.933	0.52

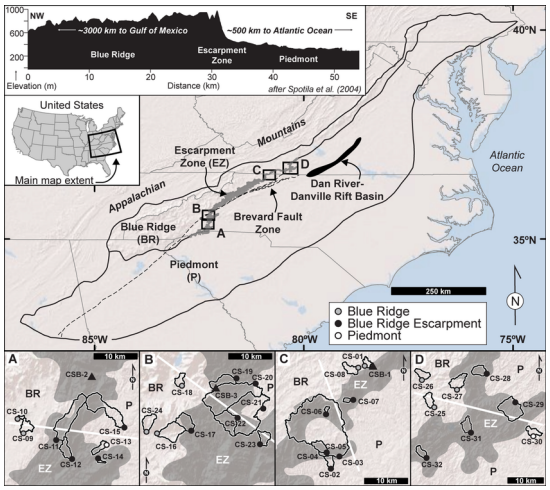

ESP_4051_F1.tif

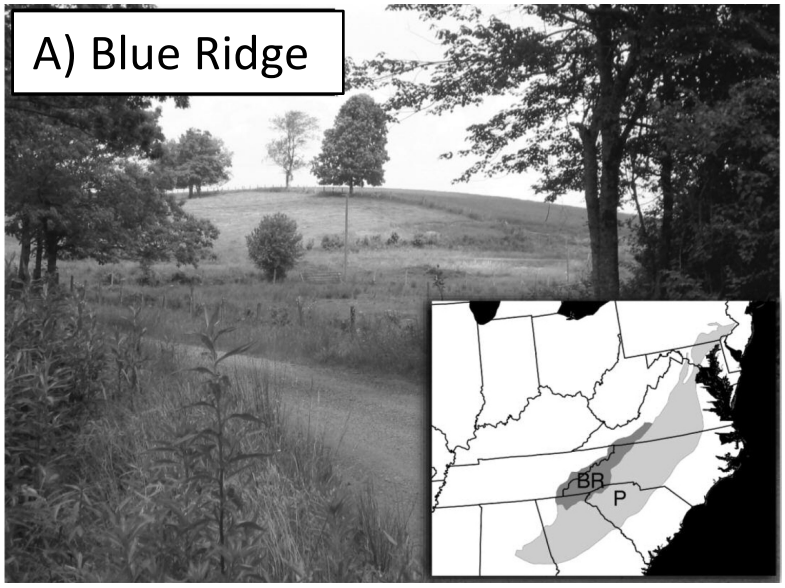

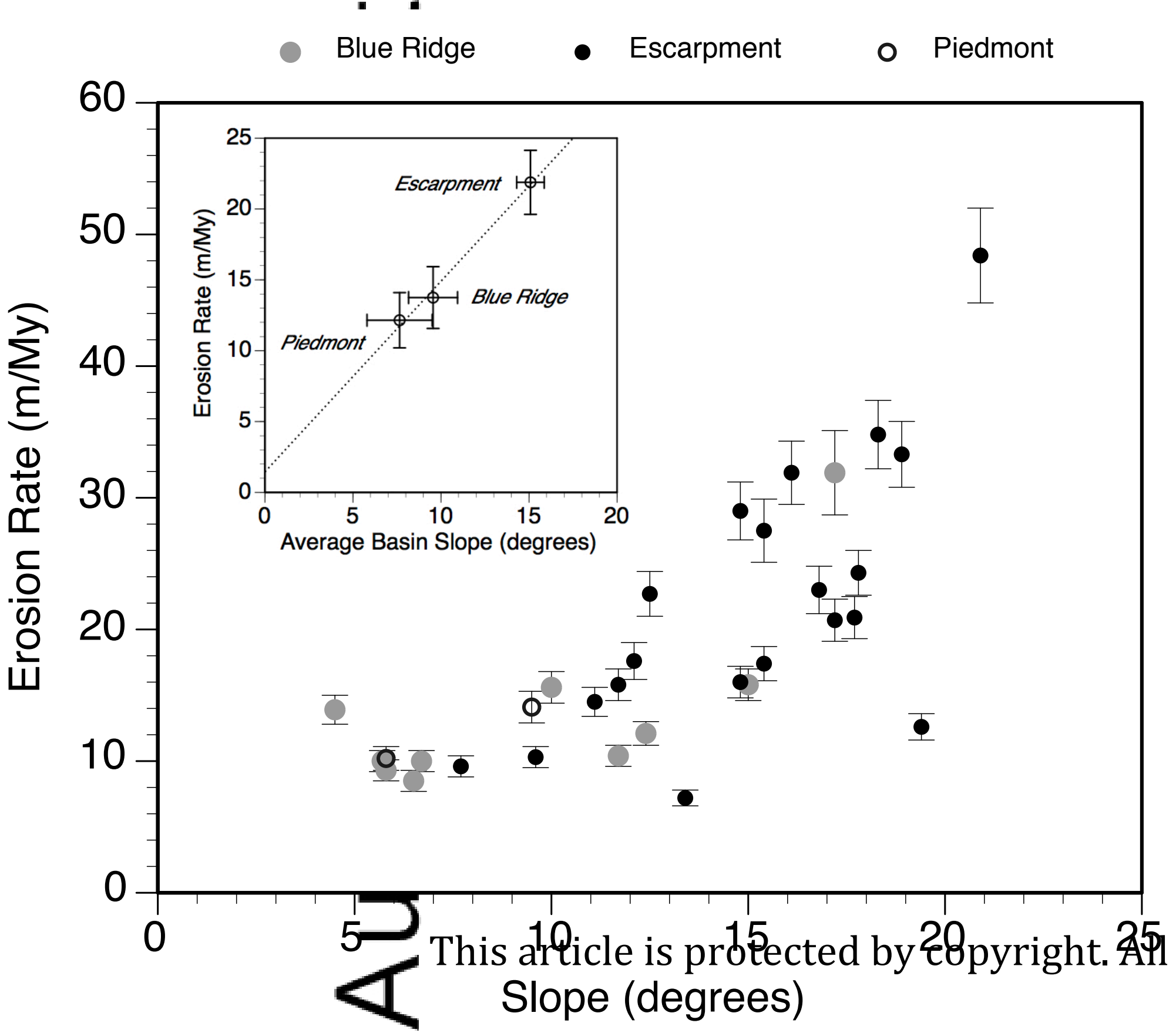

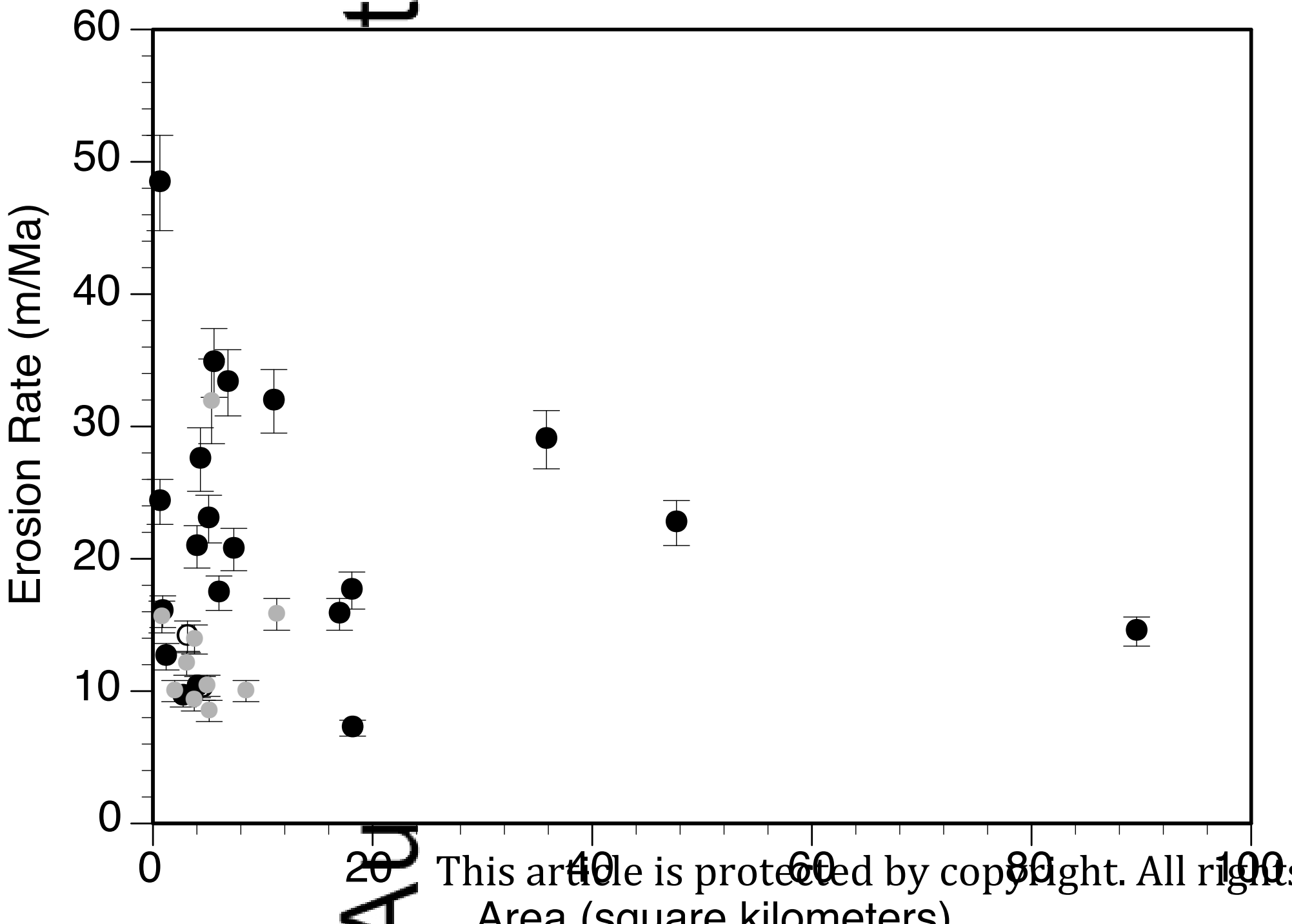

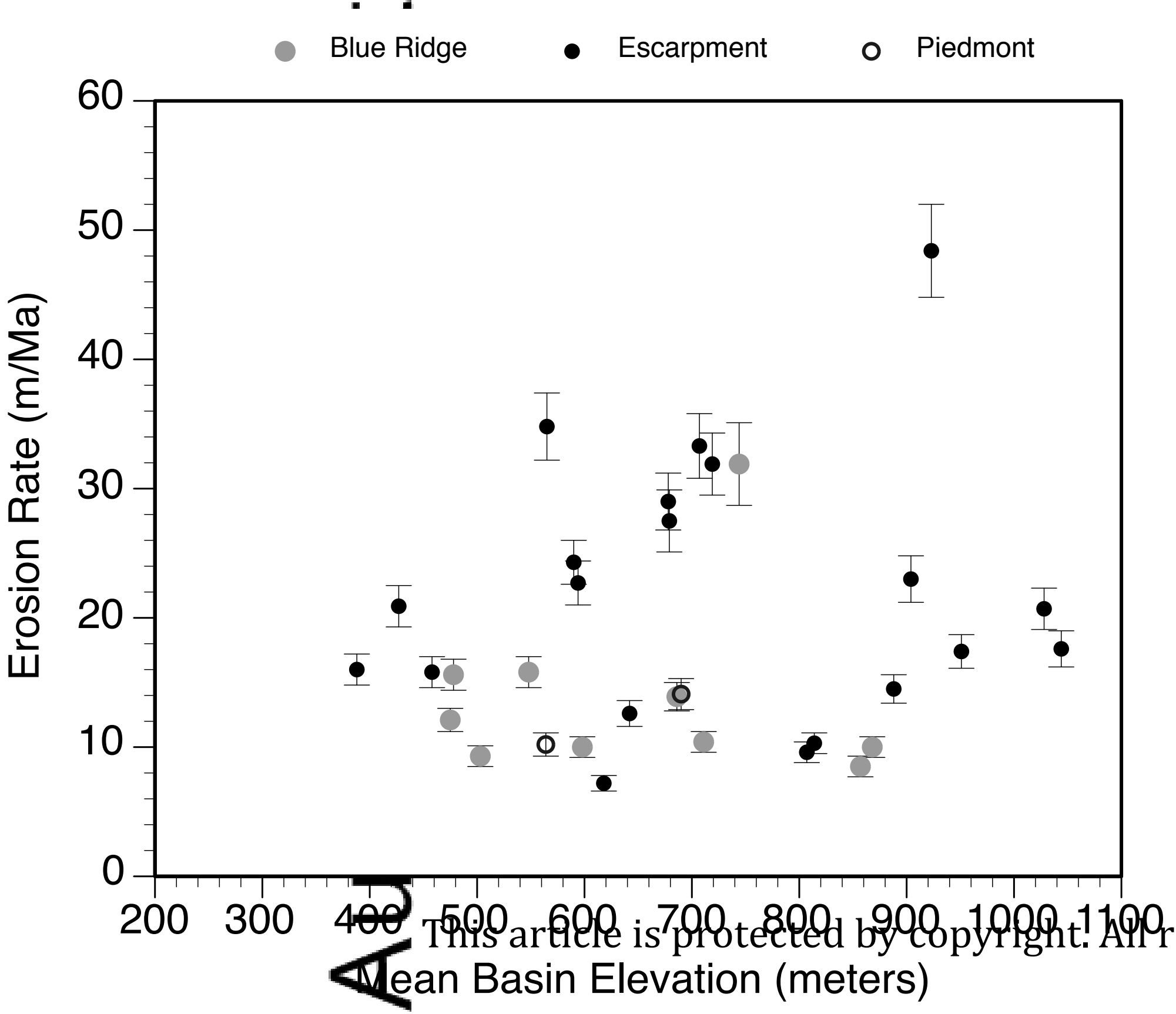

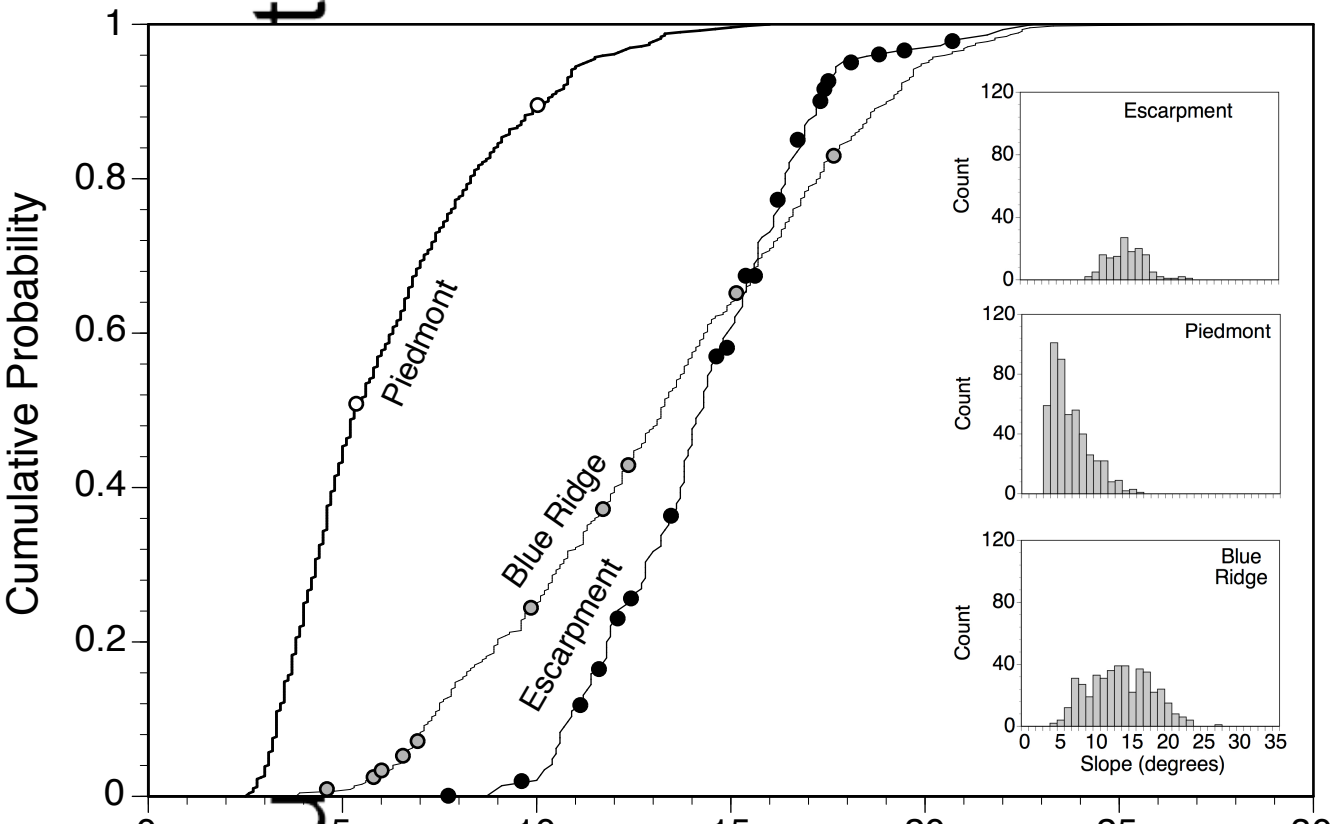

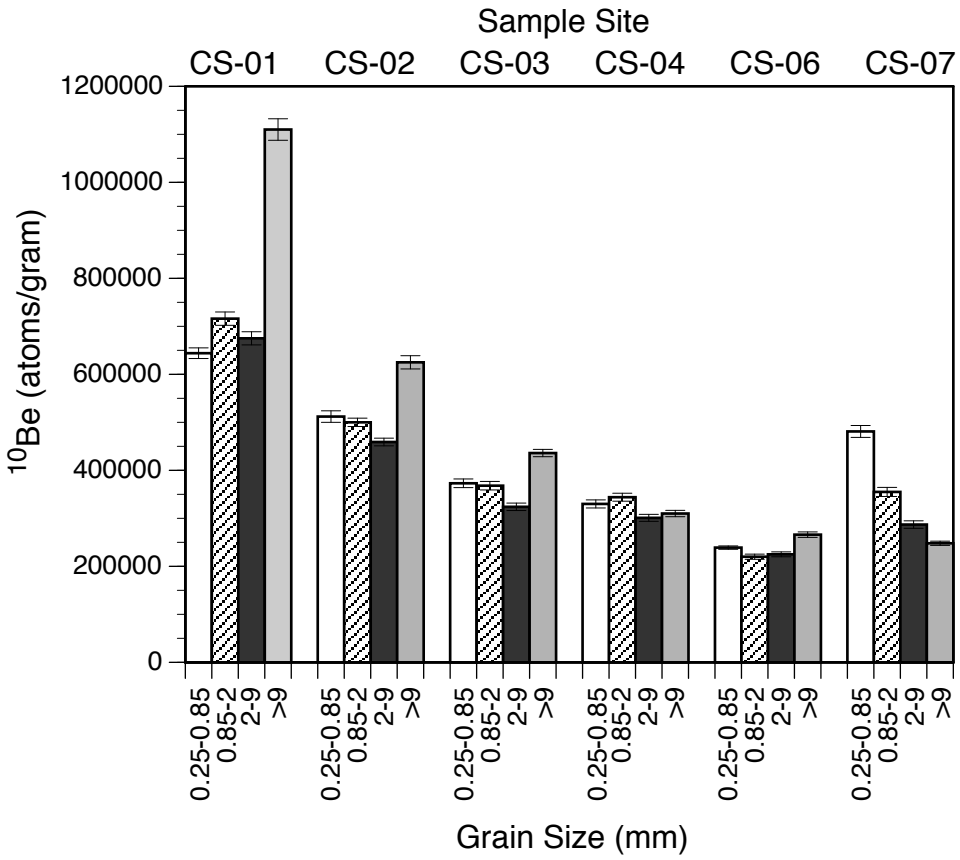

needs GIS done, not included in Portenga and Bierman

Needs CRONUS run. These are SUERC replicates

Needs careful map and GIS check because large diffrerence in basin size

Table 1. Sample information

Sample	Grain size (mm)	^{9}Be carrier (micrograms)	Quartz (grams)	Sample ID	Blank corrected ^{10}Be/^{9}Be	Measured ^{10}Be (atoms/g)	Latitude	Longitude	Relief (m)	Area (km^2)	CS AREA	Mean Latitude	Mean Longitude	Effective Elevation (m)d (m)	Slope (degrees)	CS Slope	MAP (mm)	MAT (C)	% Vegetationg (%)	CRONUS Erosion Rate m/My
CS-01	0.25-0.85	304	37.13	BE22565	1.18E-12 ± 2.03E-14	6.44E+05 ± 1.11E+04	36.61758	-80.77834	91	2.1	2.0	36.626	-80.773	867	4.8	9.0	1182	10.0	80	9.9 ± 0.8
	0.85-2	305	39.27	BE22566	1.38E-12 ± 2.67E-14	7.16E+05 ± 1.39E+04														8.8 ± 0.7
	2-9	304	40.09	BE22567	1.33E-12 ± 2.70E-14	6.75E+05 ± 1.37E+04														9.4 ± 0.8
	>9	303	35.36	BE22568	1.95E-12 ± 3.91E-14	1.11E+06 ± 2.24E+04														5.4 ± 0.5
CS-02	0.25-0.85	300	40.93	BE22581	1.05E-12 ± 2.46E-14	5.12E+05 ± 1.20E+04	36.44589	-80.84823	181	2.8	3.0	36.46	-80.851	476	6.2	12.0	1177	12.0	80	9.6 ± 0.8
	0.85-2	307	40.06	BE22582	9.77E-13 ± 1.70E-14	5.00E+05 ± 8.70E+03														9.8 ± 0.8
	2-9	299	40.02	BE22583	9.20E-13 ± 1.60E-14	4.59E+05 ± 8.01E+03														10.8 ± 0.9
	>9	306	39.40	BE22584	1.20E-12 ± 2.66E-14	6.25E+05 ± 1.38E+04														7.6 ± 0.6
CS-03	0.25-0.85	303	32.80	BE22569	6.04E-13 ± 1.46E-14	3.73E+05 ± 9.01E+03	36.46596	-80.83410	645	89.7	21.0	36.518	-80.872	557	9.5	13.0	1165	11.5	76	14.4 ± 1.2
	0.85-2	304	37.83	BE22570	6.85E-13 ± 1.65E-14	3.68E+05 ± 8.86E+03														14.6 ± 1.2
	2-9	300	40.11	BE22571	6.49E-13 ± 1.56E-14	3.24E+05 ± 7.77E+03														16.8 ± 1.3
	>9	303	40.06	BE22585	8.62E-13 ± 1.51E-14	4.36E+05 ± 7.62E+03														12.1 ± 1.0
CS-04	0.25-0.85	252	22.44	BE22533	4.39E-13 ± 1.12E-14	3.30E+05 ± 8.41E+03	36.47214	-80.85835	226	0.9	1.0	36.472	-80.865	502	13.4	19.0	1170	12.0	80	15.8 ± 1.3
	0.85-2	253	29.74	BE22534	6.07E-13 ± 1.46E-14	3.44E+05 ± 8.29E+03														15.1 ± 1.2
	2-9	252	31.27	BE22535	5.59E-13 ± 1.35E-14	3.01E+05 ± 7.27E+03														17.5 ± 1.4
	>9	252	33.61	BE22536	6.19E-13 ± 1.32E-14	3.10E+05 ± 6.62E+03														17.0 ± 1.3
CS-05	0.25-0.85	305	40.10	BE22586	9.45E-13 ± 2.33E-14	4.80E+05 ± 1.18E+04	36.47361	-80.85886	265	4.1	4.0	36.485	-80.871	477	8.4	13.0	1164	12.0	78	10.3 ± 0.8
CS-06	0.25-0.85	251	40.69	BE22541	5.81E-13 ± 8.53E-15	2.39E+05 ± 3.51E+03	36.53936	-80.86036	318	0.5	0.5	36.547	-80.859	599	16.6	22.0	1148	12.0	80	24.1 ± 1.8
	0.85-2	253	40.15	BE22542	5.22E-13 ± 1.28E-14	2.20E+05 ± 5.40E+03														26.3 ± 2.0
	2-9	253	24.84	BE22543	3.31E-13 ± 7.49E-15	2.25E+05 ± 5.10E+03														25.7 ± 2.0
	>9	253	20.61	BE22544	3.24E-13 ± 6.93E-15	2.66E+05 ± 5.68E+03														21.5 ± 1.7
CS-07	0.25-0.85	303	29.74	[illegible]	7.06E-13 ± 1.82E-14	4.81E+05 ± 1.24E+04	36.55592	-80.79931	582	1.0	1.0	36.562	-80.812	737	17.9	21.0	1184	11.0	80	12.4 ± 1.0
	0.85-2	301	24.17	[illegible]	4.27E-13 ± 1.14E-14	3.55E+05 ± 9.45E+03														17.3 ± 1.4
	2-9	302	[illegible]	[illegible]	3.37E-13 ± 9.17E-15	2.87E+05 ± 7.81E+03														21.7 ± 1.7
	>9	307	31.13	BE22552	3.76E-13 ± 6.69E-15	2.48E+05 ± 4.40E+03														25.4 ± 1.9
CS-08	0.25-0.85	314	24.47	BE22587	7.96E-13 ± 1.89E-14	6.82E+05 ± 1.62E+04	36.55225	-80.79125	151	3.7	4.0	36.615	-80.807	857	4.8	8.0	1179	10.0	63	9.2 ± 0.8
CS-09	0.25-0.85	411	28.26	BE23185	4.28E-13 ± 8.92E-15	4.16E+05 ± 8.67E+03	35.33023	-82.39133	90	4.2	4.0	35.344	-82.386	684	3.3	11.0	1395	12.0	40	13.7 ± 1.1
CS-10	0.25-0.85	408	26.98	BE23186	3.74E-13 ± 8.10E-15	3.78E+05 ± 8.19E+03	35.35671	-82.40110	86	0.6	0.7	35.359	-82.396	715	7.5	4.0	1372	12.0	62	15.6 ± 1.2
CS-11	0.25-0.85	244	[illegible]	b2276	4.47E-13 ± 1.04E-14	3.56E+05 ± 8.32E+03														±
CS-12	0.25-0.85	247	[illegible]	[illegible]	3.39E-13 ± 1.14E-14	2.52E+05 ± 8.50E+03														±
CS-13	0.25-0.85	405	[illegible]	[illegible]	3.13E-13 ± 1.15E-14	3.39E+05 ± 1.25E+04	35.31113	-82.22093	252	3.1	3.0	35.308	-82.234	391	7.7	10.0	1399	14.0	75	14.0 ± 1.2
CS-14	0.25-0.85	304	34.74	[illegible]	2.06E-13 ± 6.15E-15	1.21E+05 ± 3.61E+03	35.29235	-82.23368	505	0.7	0.7	35.287	-82.229	594	18.0	22.0	1422	14.0	80	48.7 ± 3.6
CS-14 (rep)	0.25-0.86	245	10.60	b2278	1.84E-13 ± 5.94E-15	2.84E+05 ± 9.17E+03														±
CS-15	0.25-0.85	303	34.67	[illegible]	5.49E-13 ± 1.11E-14	3.21E+05 ± 6.49E+03	35.33987	-82.18210	706	17.6	18.0	35.374	-82.222	462	9.7	12.5	1375	13.4	73	15.6 ± 1.2
CS-16	0.25-0.85	303	[illegible]	[illegible]	8.37E-13 ± 1.60E-14	4.22E+05 ± 8.07E+03	35.54200	-82.38099	559	11.1	11.0	35.545	-82.352	886	13.7	18.5	1363	11.1	78	15.6 ± 1.2
CS-17	0.25-0.85	248	[illegible]	[illegible]	2.27E-13 ± 6.69E-15	1.55E+05 ± 4.57E+03														±
CS-18	0.25-0.85	304	[illegible]	[illegible]	[illegible] ± 1.54E-14	5.13E+05 ± 9.84E+03	35.62108	-82.33010	361	3.3	3.6	35.633	-82.335	814	11.1	13.0	1317	11.2	77	12.0 ± 1.0
CS-19	0.25-0.85	304	30.35	BE23193	2.81E-13 ± 7.42E-15	1.88E+05 ± 4.96E+03	35.63589	-82.21872	496	6.4	7.0	35.632	-82.244	705	16.2	24.0	1316	11.7	80	33.0 ± 2.5
CS-20	0.25-0.85	303	26.45	BE23213	2.76E-13 ± 8.59E-15	2.11E+05 ± 6.57E+03	35.62050	-82.17887	648	35.1	35.0	35.606	-82.233	685	12.7	19.0	1323	12.1	78	28.8 ± 2.3
CS-21	0.25-0.85	309	40.90	BE23194	4.96E-13 ± 1.02E-14	2.51E+05 ± 5.16E+03	35.58390	-82.16439	619	47.4	46.0	35.574	-82.203	598	10.7	15.0	1310	12.5	79	22.5 ± 1.7
CS-22	0.25-0.85	304	29.06	BE23208	2.82E-13 ± 7.81E-15	1.97E+05 ± 5.46E+03	35.56864	-82.21732	565	10.4	10.6	35.563	-82.235	722	14.7	19.0	1332	11.9	80	31.7 ± 2.5
CS-23	0.25-0.85	[illegible]	[illegible]	[illegible]	4.32E-13 ± 2.30E-14	2.21E+05 ± 1.18E+04	35.52460	-82.16754	517	4.0	4.5	35.536	-82.160	683	13.7	18.5	1369	12.2	80	27.3 ± 2.5
CS-24	0.25-0.85	[illegible]	[illegible]	[illegible]	2.78E-13 ± 7.25E-15	2.26E+05 ± 5.89E+03	35.54752	-82.40505	579	5.1	5.3	35.563	-82.400	1064	16.4	21.0	1491	10.1	80	34.2 ± 2.7
CS-24 (rep)	0.25-0.86	247	22.60	b2280	3.51E-13 ± 9.60E-15	2.56E+05 ± 7.01E+03														±
CS-25	0.25-0.85	307	35.91	BE23197	1.33E-12 ± 4.98E-14	7.61E+05 ± 2.85E+04	36.71721	-80.43290	164	5.3	5.0	36.731	-80.443	902	5.5	10.0	1204	10.0	75	8.5 ± 0.8
CS-26	0.25-0.85	303	20.03	BE23215	6.36E-13 ± 1.37E-14	6.43E+05 ± 1.39E+04	36.77379	-80.46303	374	4.8	5.0	36.784	-80.461	923	10.6	15.0	1186	9.8	79	10.4 ± 0.9
CS-27	0.25-0.85	306	32.03	BE23209	1.06E-12 ± 3.01E-14	6.80E+05 ± 1.93E+04	36.76028	-80.37187	157	8.5	9.0	36.769	-80.370	951	5.7	10.0	1209	9.9	62	9.9 ± 0.9
CS-28	0.25-0.85	304	21.64	BE23210	3.53E-13 ± 9.82E-15	3.31E+05 ± 9.21E+03	36.78540	-80.29819	541	6.2	6.0	36.791	-80.317	626	14.2	19.0	1203	11.1	80	17.3 ± 1.4
CS-29	0.25-0.85	301	[illegible]	BE23198	1.35E-12 ± 2.64E-14	7.04E+05 ± 1.38E+04	36.72536	-80.22598	545	18.2	5.0	36.713	-80.236	571	11.2	21.0	1255	11.7	76	7.2 ± 0.6
CS-30	0.25-0.85	304	[illegible]	[illegible]	9.53E-13 ± 4.67E-14	4.83E+05 ± 2.37E+04	36.65900	-80.17998	193	4.5	4.5	36.667	-80.181	427	4.8	9.0	1252	12.0	76	9.9 ± 0.9
CS-30 (rep)	0.25-0.86	247	[illegible]	[illegible]	5.60E-13 ± 2.88E-14	4.70E+05 ± 2.42E+04														±
CS-31	0.25-0.85	307	32.12	BE23200	2.84E-13 ± 8.37E-15	1.81E+05 ± 5.33E+03	36.66414	-80.34017	399	5.5	5.5	36.68	-80.348	690	16.3	23.0	1236	10.9	79	34.5 ± 2.6
CS-32	0.25-0.85	306	34.91	BE23211	4.60E-13 ± 1.07E-14	2.69E+05 ± 6.26E+03	36.61564	-80.45112	645	116.4	10.0	36.702	-80.409	833	9.1	24.0	1217	10.2	75	24.9 ± 1.9
CSB-1	NA	304	26.40	BE23201	8.94E-14 ± 5.24E-15	6.88E+04 ± 4.03E+03	36.620	-80.760												105.87 ± 9.39
CSB-2	NA	303	[illegible]	[illegible]	1.75E-12 ± 3.54E-14	2.71E+06 ± 5.48E+04	35.430	-82.250												1.48 ± 0.16
CSB-3	NA	303	[illegible]	[illegible]	4.73E-13 ± 1.68E-14	3.34E+05 ± 1.19E+04	35.620	-82.260												20.62 ± 1.74

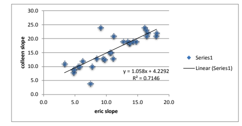

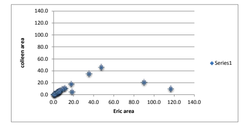

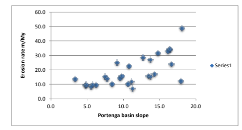

Sample ID	Grain Size (mm)	9Be Carrier (ug)	Quartz (g)	BE #	Blank Corrected 9Be/10Be	Meas. 10Be (atoms/g)	Lat (dd)	long (dd)	Mean Lat	Mean Long	Elev (m)	Eff Elev (m)	Area (km2)	%BRE	Province	Relief	Mean Slope (°)	Median Slope (°)	CRONUS Erate (m/Myr)	
CS-01	0.25-0.85	304	37.13	BE22565	1.18E-12 ± 2.03E-14	644000 ± 11100	36.6206	-80.7778	36.6258	-80.7728	867.6	867.8	1.98	6	BR	93	5.7	5	9.97 ± 0.78	CS-01
CS-01	0.85-2	305	39.27	BE22566	1.38E-12 ± 2.67E-14	716000 ± 13900	36.6206	-80.7778	36.6258	-80.7728	867.6	867.8	1.98	6	BR	93	5.7	5	8.87 ± 0.71	CS-01
CS-01	2-9	304	40.09	BE22567	1.33E-12 ± 2.70E-14	675000 ± 13700	36.6206	-80.7778	36.6258	-80.7728	867.6	867.8	1.98	6	BR	93	5.7	5	9.47 ± 0.76	CS-01
CS-01	>9	303	35.36	BE22568	1.95E-12 ± 3.91E-14	1110000 ± 22400	36.6206	-80.7778	36.6258	-80.7728	867.6	867.8	1.98	6	BR	93	5.7	5	5.44 ± 0.46	CS-01
CS-02	0.25-0.85	300	40.93	BE22581	1.05E-12 ± 2.46E-14	512000 ± 12000	36.4478	-80.8480	36.4603	-80.8505	478.0	478.2	2.75	52	BRE	191	7.7	7	9.63 ± 0.76	CS-02
CS-02	0.85-2	307	40.06	BE22582	9.77E-13 ± 1.70E-14	500000 ± 8700	36.4478	-80.8480	36.4603	-80.8505	478.0	478.2	2.75	52	BRE	191	7.7	7	9.89 ± 0.76	CS-02
CS-02	2-9	299	40.02	BE22583	9.20E-13 ± 1.60E-14	459000 ± 8010	36.4478	-80.8480	36.4603	-80.8505	478.0	478.2	2.75	52	BRE	191	7.7	7	10.88 ± 0.83	CS-02
CS-02	>9	306	39.40	BE22584	1.20E-12 ± 2.66E-14	625000 ± 13800	36.4478	-80.8480	36.4603	-80.8505	478.0	478.2	2.75	52	BRE	191	7.7	7	7.7 ± 0.62	CS-02
CS-03	0.25-0.85	303	32.80	BE22569	6.04E-13 ± 1.46E-14	373000 ± 9010	36.4683	-80.8305	36.5186	-80.8718	548.3	558.4	89.57	62	BRE	662	11.1	9	14.52 ± 1.11	CS-03
CS-03	0.85-2	304	37.83	BE22570	6.85E-13 ± 1.65E-14	368000 ± 8860	36.4683	-80.8305	36.5186	-80.8718	548.3	558.4	89.57	62	BRE	662	11.1	9	14.74 ± 1.13	CS-03
CS-03	2-9	300	40.11	BE22571	6.49E-13 ± 1.56E-14	324000 ± 7770	36.4683	-80.8305	36.5186	-80.8718	548.3	558.4	89.57	62	BRE	662	11.1	9	16.95 ± 1.28	CS-03
CS-03	>9	303	40.06	BE22585	8.62E-13 ± 1.51E-14	436000 ± 7620	36.4683	-80.8305	36.5186	-80.8718	548.3	558.4	89.57	62	BRE	662	11.1	9	12.23 ± 0.93	CS-03
CS-04	0.25-0.85	252	22.44	BE22533	4.39E-13 ± 1.12E-14	330000 ± 8410	36.4747	-80.8572	36.4722	-80.8656	503.4	505.1	0.89	100	BRE	238	14.8	14	15.99 ± 1.22	CS-04
CS-04	0.85-2	253	29.74	BE22534	6.07E-13 ± 1.46E-14	344000 ± 8290	36.4747	-80.8572	36.4722	-80.8656	503.4	505.1	0.89	100	BRE	238	14.8	14	15.27 ± 1.16	CS-04
CS-04	2-9	252	31.27	BE22535	5.59E-13 ± 1.35E-14	301000 ± 7270	36.4747	-80.8572	36.4722	-80.8656	503.4	505.1	0.89	100	BRE	238	14.8	14	17.68 ± 1.33	CS-04
CS-04	>9	252	33.61	BE22536	6.19E-13 ± 1.32E-14	310000 ± 6620	36.4747	-80.8572	36.4722	-80.8656	503.4	505.1	0.89	100	BRE	238	14.8	14	17.12 ± 1.27	CS-04
CS-05	0.25-0.85	305	40.10	BE22586	9.45E-13 ± 2.33E-14	480000 ± 11800	36.4750	-80.8572	36.4848	-80.8710	474.7	475.4	4.06	78	BRE	269	9.6	8	10.34 ± 0.82	CS-05
CS-06	0.25-0.85	251	40.69	BE22541	5.81E-13 ± 8.53E-15	239000 ± 3510	36.5391	-80.8583	36.5468	-80.8575	597.9	601.2	0.64	100	BRE	364	17.8	18	24.29 ± 1.73	CS-06
CS-06	0.85-2	253	40.15	BE22542	5.22E-13 ± 1.28E-14	220000 ± 5400	36.5391	-80.8583	36.5468	-80.8575	597.9	601.2	0.64	100	BRE	364	17.8	18	26.55 ± 1.95	CS-06
CS-06	2-9	253	24.84	BE22543	3.31E-13 ± 7.49E-15	225000 ± 5100	36.5391	-80.8583	36.5468	-80.8575	597.9	601.2	0.64	100	BRE	364	17.8	18	25.92 ± 1.89	CS-06
CS-06	>9	253	20.61	BE22544	3.24E-13 ± 6.93E-15	266000 ± 5680	36.5391	-80.8583	36.5468	-80.8575	597.9	601.2	0.64	100	BRE	364	17.8	18	21.64 ± 1.59	CS-06
CS-07	0.25-0.85	303	29.74	BE22549	7.06E-13 ± 1.82E-14	481000 ± 12400	36.5611	-80.7995	36.5629	-80.8131	744.2	754.1	1.20	98	BRE	600	19.4	18	12.64 ± 1	CS-07
CS-07	0.85-2	[illegible]	24.17	BE22550	4.27E-13 ± 1.14E-14	355000 ± 9450	36.5611	-80.7995	36.5629	-80.8131	744.2	754.1	1.20	98	BRE	600	19.4	18	17.59 ± 1.36	CS-07
CS-07	2-9	302	23.66	BE22551	3.37E-13 ± 9.17E-15	287000 ± 7810	36.5611	-80.7995	36.5629	-80.8131	744.2	754.1	1.20	98	BRE	600	19.4	18	22.13 ± 1.69	CS-07
CS-07	>9	307	31.13	BE22552	3.76E-13 ± 6.69E-15	248000 ± 4400	36.5611	-80.7995	36.5629	-80.8131	744.2	754.1	1.20	98	BRE	600	19.4	18	25.88 ± 1.88	CS-07
CS-08	0.25-0.85	314	24.47	BE22587	7.96E-13 ± 1.89E-14	682000 ± 16200	36.6176	-80.7911	36.6153	-80.8072	856.9	856.9	3.76	6	BR	154	5.8	5	9.29 ± 0.75	CS-08
CS-09	0.25-0.85	[illegible]86	BE23185	4.28E-13 ± 8.92E-15	416000 ± 8670	35.3335	-82.3925	35.3454	-82.3855	686.3	686.9	3.78	0	BR	91	4.5	4	13.85 ± 1.06	CS-09
CS-10	0.25-0.85	408	26.98	BE23186	3.74E-13 ± 8.10E-15	378000 ± 8187	35.3578	-82.4050	35.3599	-82.3983	710.7	711.1	0.81	0	BR	107	10	10	15.64 ± 1.19	CS-10
CS-11	0.25-0.85	244	20.48	b2276	4.47E-13 ± 1.04E-14	356193 ± 8317	35.3216	-82.3242	35.3589	-82.2974	807.2	810.0	18.11	83	BRE	522	12.1	11	17.85 ± 1.36	CS-11
CS-12	0.25-0.85	247	22.18	b2277	3.39E-13 ± 1.14E-14	251928 ± 8497	35.2889	-82.2911	35.3057	-82.3041	642.2	648.7	5.07	100	BRE	571	16.8	16	23.25 ± 1.82	CS-12
CS-13	0.25-0.85	405	25.01	BE23187	3.13E-13 ± 1.15E-14	339000 ± 12455	35.3133	-82.2189	35.3081	-82.2339	388.4	390.1	3.14	49	PIED	268	9.5	8	14.08 ± 1.15	CS-13
CS-14	0.25-0.85	304	34.74	BE23189	2.06E-13 ± 6.15E-15	121000 ± 3612	35.2942	-82.2331	35.2869	-82.2286	590.3	598.6	0.63	100	BRE	518	20.9	20	49.2 ± 3.59	CS-14
CS-14 (rep)	0.25-0.86	245	24.34	b2278	1.84E-13 ± 5.94E-15	283978 ± 9169	35.2942	-82.2331	35.2869	-82.2286	590.3	598.6	0.63	100	BRE	518	20.9	20	17.7 ± 1.39	CS-14 (rep)
CS-15	0.25-0.85	[illegible]	34.67	BE23190	5.49E-13 ± 1.11E-14	321000 ± 6490	35.3425	-82.1818	35.3749	-82.2238	458.4	467.0	16.99	51	BRE	722	11.7	10	15.8 ± 1.17	CS-15
CS-16	0.25-0.85	303	40.10	BE23191	8.37E-13 ± 1.60E-14	422000 ± 8067	35.5419	-82.3828	35.5452	-82.3522	887.6	892.4	11.27	0	BR	569	15	15	15.77 ± 1.2	CS-16
CS-17	0.25-0.85	248	10.57	b2279	2.27E-13 ± 6.69E-15	154686 ± 4565	35.5480	-82.3113	35.5619	-82.3236	1028.1	1033.3	7.36	82	BRE	513	17.2	17	50.21 ± 3.79	CS-17
CS-18	0.25-0.85	305	31.82	BE23192	8.03E-13 ± 1.54E-14	513000 ± 9838	35.6236	-82.3311	35.6332	-82.3350	814.4	815.9	3.07	0	BR	389	12.4	12	12.11 ± 0.94	CS-18
CS-19	0.25-0.85	304	30.35	BE23193	2.81E-13 ± 7.42E-15	188000 ± 4964	35.6361	-82.2178	35.6315	-82.2451	707.3	711.6	6.83	100	BRE	520	18.9	19	33.32 ± 2.46	CS-19
CS-20	0.25-0.85	303	26.45	BE23213	2.76E-13 ± 8.59E-15	211000 ± 6567	35.6253	-82.1761	35.6062	-82.2328	677.9	686.2	35.83	89	BRE	655	14.8	15	28.97 ± 2.21	CS-20
CS-21	0.25-0.85	[illegible]	40.90	BE23194	4.96E-13 ± 1.02E-14	251000 ± 5162	35.5848	-82.1606	35.5741	-82.2031	593.7	599.3	47.67	68	BRE	624	12.5	11	22.68 ± 1.65	CS-21
CS-22	0.25-0.85	304	29.06	BE23208	2.82E-13 ± 7.81E-15	197000 ± 5456	35.5692	-82.2147	35.5628	-82.2355	718.5	723.2	11.01	100	BRE	573	16.1	15	31.91 ± 2.38	CS-22
CS-23	0.25-0.85	306	40.02	BE23195	4.32E-13 ± 2.30E-14	221000 ± 11766	35.5244	-82.1678	35.5349	-82.1587	679.1	682.2	4.32	100	BRE	548	15.4	15	27.46 ± 2.44	CS-23
CS-24	0.25-0.85	[illegible]	25.00	BE23214	2.78E-13 ± 7.25E-15	226000 ± 5894	35.5455	-82.4053	35.5622	-82.4006	1043.7	1051.3	5.34	0	BR	609	17.2	18	34.14 ± 2.58	CS-24
CS-24 (rep)	0.25-0.86	247	22.64	b2280	3.51E-13 ± 9.60E-15	256493 ± 7012	35.5455	-82.4053	35.5622	-82.4006	1043.7	1051.3	5.34	0	BR	609	17.2	18	26.85 ± 2.07	CS-24 (rep)
CS-25	0.25-0.85	307	35.91	BE23197	1.33E-12 ± 4.98E-14	761000 ± 28495	36.7172	-80.4313	36.7316	-80.4433	903.5	904.0	5.12	0	BR	175	6.5	6	8.54 ± 0.75	CS-25
CS-26	0.25-0.85	3[illegible]	20.03	BE23215	6.36E-13 ± 1.37E-14	643000 ± 13851	36.7727	-80.4625	36.7843	-80.4609	922.6	924.7	4.93	0	BR	390	11.7	11	10.44 ± 0.83	CS-26
CS-27	0.25-0.85	306	32.03	BE23209	1.06E-12 ± 3.01E-14	680000 ± 19309	36.7533	-80.3731	36.7690	-80.3704	951.0	951.7	8.47	29	BR	159	6.7	6	10.01 ± 0.83	CS-27
CS-28	0.25-0.85	304	21.64	BE23210	3.53E-13 ± 9.82E-15	331000 ± 9208	36.7856	-80.2980	36.7917	-80.3168	618.4	623.2	6.01	100	BRE	546	15.4	15	17.39 ± 1.34	CS-28
CS-29	0.25-0.85	[illegible]	38.42	BE23198	1.35E-12 ± 2.64E-14	704000 ± 13767	36.7275	-80.2253	36.7134	-80.2363	564.8	568.4	18.18	85	BRE	548	13.4	12	7.24 ± 0.58	CS-29
CS-30	0.25-0.85	304	40.05	BE23199	9.53E-13 ± 4.67E-14	483000 ± 23669	36.6587	-80.1800	36.6674	-80.1805	427.4	427.5	4.51	1	PIED	194	5.8	5	9.93 ± 0.91	CS-30
CS-30 (rep)	0.25-0.86	247	19.74	b2283	5.60E-13 ± 2.88E-14	469743 ± 24162	36.6587	-80.1800	36.6674	-80.1805	427.4	427.5	4.51	1	PIED	194	5.8	5	9.15 ± 0.86	CS-30 (rep)
CS-31	0.25-0.85	307	32.12	BE23200	2.84E-13 ± 8.37E-15	181000 ± 5334	36.6655	-80.3384	36.6802	-80.3479	689.9	693.7	5.56	100	BRE	400	18.3	19	34.84 ± 2.61	CS-31
CS-32	0.25-0.85	306	34.91	BE23211	4.60E-13 ± 1.07E-14	269000 ± 6257	36.6142	-80.4505	36.6258	-80.4638	563.7	569.3	4.01	100	BRE	449	17.7	17	20.94 ± 1.55	CS-32
CSB-1	NA	304	26.40	BE23201	8.94E-14 ± 5.24E-15	68800 ± 4033	36.6200	-80.7600			892.0								106.27 ± 9.48	CSB-1
CSB-2	NA	303	13.08	BE23216	1.75E-12 ± 3.54E-14	2710000 ± 54819	35.4300	-82.2500			694.0								1.54 ± 0.16	CSB-2
CSB-3	NA	[illegible]	28.71	BE23202	4.73E-13 ± 1.68E-14	334000 ± 11863	35.6200	-82.2600			957.0								20.77 ± 1.68	CSB-3

CS 30 has low llnl current (2 uA compared ot others, teens)
external unc

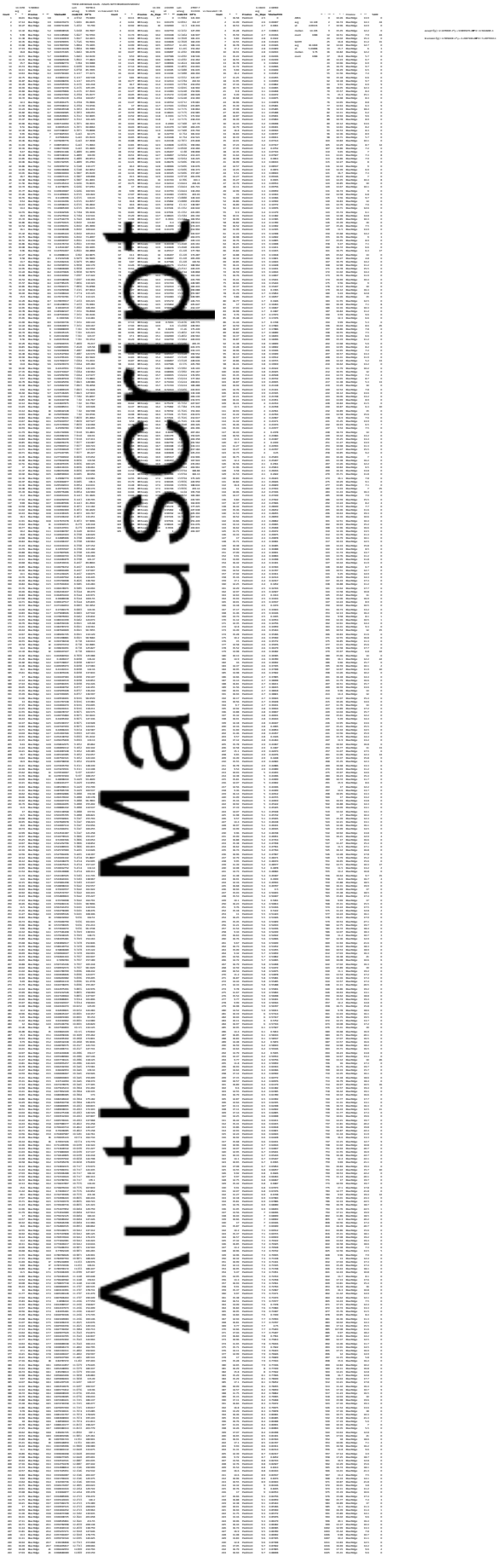

Sample ID	Lat (dd)	Long (dd)	Elev (m)	Press. Flag	Thickness (cm)	Denisty (g/cm3)	Shielding	[10Be]	[10Be] err	10Be STD	[26Al]	[26Al] err	26Al STD
CS-01_250-850	36.6258	-80.7728	867.8	std	0.01	2.7	1	644000	11100	KNSTD	0	0	0
CS-01_850-2k	36.6258	-80.7728	867.8	std	0.01	2.7	1	716000	13900	KNSTD	0	0	0
CS-01_2k-9k	36.6258	-80.7728	867.8	std	0.01	2.7	1	675000	13700	KNSTD	0	0	0
CS-01_GT9k	36.6258	-80.7728	867.8	std	0.01	2.7	1	1110000	22400	KNSTD	0	0	0
CS-02_250-850	36.4603	-80.8505	478.2	std	0.01	2.7	1	512000	12000	KNSTD	0	0	0
CS-02_850-2k	36.4603	-80.8505	478.2	std	0.01	2.7	1	500000	8700	KNSTD	0	0	0
CS-02_2k-9k	36.4603	-80.8505	478.2	std	0.01	2.7	1	459000	8010	KNSTD	0	0	0
CS-02_GT9k	36.4603	-80.8505	478.2	std	0.01	2.7	1	625000	13800	KNSTD	0	0	0
CS-03_250-850	36.5186	-80.8718	558.4	std	0.01	2.7	1	373000	9010	KNSTD	0	0	0
CS-03_850-2k	36.5186	-80.8718	558.4	std	0.01	2.7	1	368000	8860	KNSTD	0	0	0
CS-03_2k-9k	36.5186	-80.8718	558.4	std	0.01	2.7	1	324000	7770	KNSTD	0	0	0
CS-03_GT9k	36.5186	-80.8718	558.4	std	0.01	2.7	1	436000	7620	KNSTD	0	0	0
CS-04_250-850	36.4722	-80.8656	505.1	std	0.01	2.7	1	330000	8410	KNSTD	0	0	0
CS-04_850-2k	36.4722	-80.8656	505.1	std	0.01	2.7	1	344000	8290	KNSTD	0	0	0
CS-04_2k-9k	36.4722	-80.8656	505.1	std	0.01	2.7	1	301000	7270	KNSTD	0	0	0
CS-04_GT9k	36.4722	-80.8656	505.1	std	0.01	2.7	1	310000	6620	KNSTD	0	0	0
CS-05	36.4848	-80.8710	475.4	std	0.01	2.7	1	480000	11800	KNSTD	0	0	0
CS-06_250-850	36.5468	-80.8575	601.2	std	0.01	2.7	1	239000	3510	KNSTD	0	0	0
CS-06_850-2k	36.5468	-80.8575	601.2	std	0.01	2.7	1	220000	5400	KNSTD	0	0	0
CS-06_2k-9k	36.5468	-80.8575	601.2	std	0.01	2.7	1	225000	5100	KNSTD	0	0	0
CS-06_GT9k	36.5468	-80.8575	601.2	std	0.01	2.7	1	266000	5680	KNSTD	0	0	0
CS-07_250-850	36.5629	-80.8131	754.1	std	0.01	2.7	1	481000	12400	KNSTD	0	0	0
CS-07_850-2k	36.5629	-80.8131	754.1	std	0.01	2.7	1	355000	9450	KNSTD	0	0	0
CS-07_2k-9k	36.5629	-80.8131	754.1	std	0.01	2.7	1	287000	7810	KNSTD	0	0	0
CS-07_GT9k	36.5629	-80.8131	754.1	std	0.01	2.7	1	248000	4400	KNSTD	0	0	0
CS-08	36.6153	-80.8072	856.9	std	0.01	2.7	1	682000	16200	KNSTD	0	0	0
CS-09	35.3454	-82.3855	686.9	std	0.01	2.7	1	416000	8670	KNSTD	0	0	0
CS-10	35.3599	-82.3983	711.1	std	0.01	2.7	1	378000	8187	KNSTD	0	0	0
CS-11	35.3589	-82.2974	810.0	std	0.01	2.7	1	356593	8327	NIST_30600	0	0	0
CS-12	35.3057	-82.3041	648.7	std	0.01	2.7	1	252212	8507	NIST_30600	0	0	0
CS-13	35.3081	-82.2339	390.1	std	0.01	2.7	1	339000	12455	KNSTD	0	0	0
CS-14	35.2869	-82.2286	598.6	std	0.01	2.7	1	121000	3612	KNSTD	0	0	0
CS-14rep	35.2869	-82.2286	598.6	std	0.01	2.7	1	123676.6	3993.097	NIST_30600	0	0	0
CS-15	35.3749	-82.2238	467.0	std	0.01	2.7	1	321000	6490	KNSTD	0	0	0
CS-16	35.5453	-82.3522	892.4	std	0.01	2.7	1	422000	8067	KNSTD	0	0	0
CS-17	35.5019	-82.3236	1033.3	std	0.01	2.7	1	355617.2	10495.53	NIST_30600	0	0	0
CS-18	36.6312	-82.3350	815.9	std	0.01	2.7	1	513000	9838	KNSTD	0	0	0
CS-19	35.6315	-82.2451	711.6	std	0.01	2.7	1	188000	4964	KNSTD	0	0	0
CS-20	35.6002	-82.2328	686.2	std	0.01	2.7	1	211000	6567	KNSTD	0	0	0
CS-21	35.5741	-82.2031	599.3	std	0.01	2.7	1	251000	5162	KNSTD	0	0	0
CS-22	35.5629	-82.2355	723.2	std	0.01	2.7	1	197000	5456	KNSTD	0	0	0
CS-23	35.5349	-82.1587	682.2	std	0.01	2.7	1	221000	11766	KNSTD	0	0	0
CS-24	35.5622	-82.4006	1051.3	std	0.01	2.7	1	226000	5894	KNSTD	0	0	0
CS-24rep	35.5622	-82.4006	1051.3	std	0.01	2.7	1	256493	7012	NIST_30600	0	0	0
CS-25	36.7316	-80.4433	904.0	std	0.01	2.7	1	761000	28495	KNSTD	0	0	0
CS-26	36.7843	-80.4609	924.7	std	0.01	2.7	1	643000	13851	KNSTD	0	0	0
CS-27	36.7609	-80.3704	951.7	std	0.01	2.7	1	680000	19309	KNSTD	0	0	0
CS-28	36.7917	-80.3168	623.2	std	0.01	2.7	1	331000	9208	KNSTD	0	0	0
CS-29	36.7134	-80.2363	568.4	std	0.01	2.7	1	704000	13767	KNSTD	0	0	0
CS-30	36.6674	-80.1805	427.5	std	0.01	2.7	1	483000	23669	KNSTD	0	0	0
CS-30rep	36.6674	-80.1805	427.5	std	0.01	2.7	1	459390.4	24148.26	NIST_30600	0	0	0
CS-31	36.6802	-80.3479	693.7	std	0.01	2.7	1	181000	5334	KNSTD	0	0	0
CS-32	36.6258	-80.4638	569.3	std	0.01	2.7	1	269000	6257	KNSTD	0	0	0
CSB-1	36.6200	-80.7600	892.0	std	3	2.7	1	68800	4033	KNSTD	0	0	0
CSB-2	35.4300	-82.2500	694.0	std	3	2.7	1	2710000	54819	KNSTD	0	0	0
CSB-3	36.6200	-82.2600	957.0	std	3	2.7	1	334000	11863	KNSTD	0	0	0

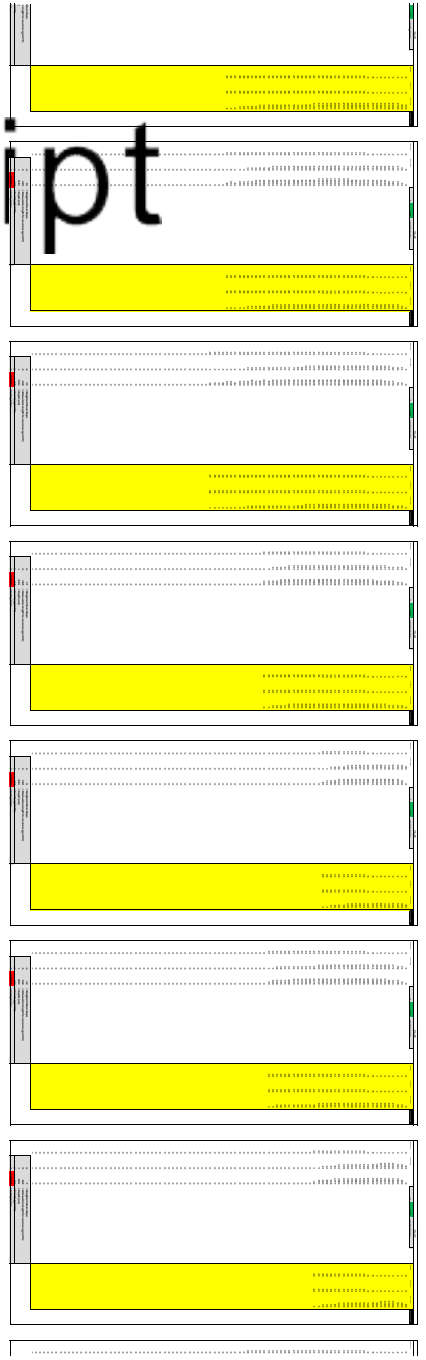

Name	shield	Production rate (muons)	Internal uncertainty (m/Myr)	Erosion rate (g/cm2/yr)	Erosion rate (m/Myr)	External uncertainty (m/Myr)	Production rate (spallation) (atoms/g/yr)
CS-01_250-85	1	0.24	0.18	0.00269	9.97	0.78	8.09
CS-01_850-2k	1	0.24	0.19	0.0024	8.87	0.71	8.09
CS-01_2k-9k	1	0.24	0.21	0.00256	9.47	0.76	8.09
CS-01_GT9k	1	0.24	0.12	0.00147	5.44	0.46	8.09
CS-02_250-85	1	0.211	0.25	0.0026	9.63	0.76	5.9
CS-02_850-2k	1	0.211	0.19	0.00267	9.89	0.76	5.9
CS-02_2k-9k	1	0.211	0.21	0.00294	10.88	0.83	5.9
CS-02_GT9k	1	0.211	0.19	0.00208	7.7	0.62	5.9
CS-03_250-85	1	0.216	0.38	0.00392	14.52	1.11	6.31
CS-03_850-2k	1	0.216	0.38	0.00398	14.74	1.13	6.31
CS-03_2k-9k	1	0.216	0.43	0.00458	16.95	1.28	6.31
CS-03_GT9k	1	0.216	0.23	0.0033	12.23	0.93	6.31
CS-04_250-85	1	0.213	0.43	0.00432	15.99	1.22	6.04
CS-04_850-2k	1	0.213	0.39	0.00412	15.27	1.16	6.04
CS-04_2k-9k	1	0.213	0.45	0.00477	17.68	1.33	6.04
CS-04_GT9k	1	0.213	0.39	0.00462	17.12	1.27	6.04
CS-05	1	0.21	0.28	0.00279	10.34	0.82	5.89
CS-06_250-85	1	0.22	0.37	0.00656	24.29	1.73	6.54
CS-06_850-2k	1	0.22	0.68	0.00717	26.55	1.95	6.54
CS-06_2k-9k	1	0.22	0.61	0.007	25.92	1.89	6.54
CS-06_GT9k	1	0.22	0.49	0.00584	21.64	1.59	6.54
CS-07_250-85	1	0.231	0.35	0.00341	12.64	1	7.39
CS-07_850-2k	1	0.231	0.49	0.00475	17.59	1.36	7.39
CS-07_2k-9k	1	0.231	0.63	0.00597	22.13	1.69	7.39
CS-07_GT9k	1	0.231	0.48	0.00699	25.88	1.88	7.39
CS-08	1	0.24	0.24	0.00251	9.29	0.75	8.02
CS-09	1	0.226	0.31	0.00374	13.85	1.06	6.84
CS-10	1	0.228	0.36	0.00422	15.64	1.19	6.97
CS-11	1	0.236	0.43	0.00476	17.64	1.35	7.53
CS-12	1	0.223	0.81	0.00621	22.98	1.8	6.63
CS-13	1	0.204	0.56	0.0038	14.08	1.15	5.38
CS-14	1	0.219	1.51	0.01328	49.2	3.59	6.37
CS-14rep	1	0.219	1.58	0.01285	47.58	3.53	6.37
CS-15	1	0.21	0.34	0.00427	15.8	1.17	5.74
CS-16	1	0.242	0.32	0.00426	15.77	1.2	8.06
CS-17	1	0.254	0.64	0.00558	20.65	1.63	8.98
CS-18	1	0.236	0.25	0.00327	12.11	0.94	7.61
CS-19	1	0.228	0.91	0.009	33.32	2.46	7.01
CS-20	1	0.226	0.94	0.00782	28.97	2.21	6.87
CS-21	1	0.219	0.49	0.00612	22.68	1.65	6.41
CS-22	1	0.229	0.92	0.00862	31.91	2.38	7.07
CS-23	1	0.226	1.53	0.00742	27.46	2.44	6.84
CS-24	1	0.255	0.92	0.00922	34.14	2.58	9.11
CS-24rep	1	0.255	0.84	0.00798	29.57	2.26	9.11
CS-25	1	0.243	0.35	0.0023	8.54	0.75	8.34
CS-26	1	0.245	0.24	0.00282	10.44	0.83	8.49
CS-27	1	0.247	0.31	0.0027	10.01	0.83	8.66
CS-28	1	0.221	0.51	0.0047	17.39	1.34	6.68
CS-29	1	0.217	0.16	0.00195	7.24	0.58	6.38
CS-30	1	0.207	0.53	0.00268	9.93	0.91	5.68
CS-30rep	1	0.207	0.6	0.00281	10.39	0.97	5.68
CS-31	1	0.227	1.06	0.00941	34.84	2.61	7.06
CS-32	1	0.217	0.51	0.00565	20.94	1.55	6.38
CSB-1	1	0.241	6.33	0.02869	106.27	9.48	8.24
CSB-2	1	0.225	0.04	0.00042	1.54	0.16	6.89
CSB-3	1	0.246	0.77	0.00561	20.77	1.68	8.49

Wrapper script: 2.2
Main calculator: 2.1
Objective function: 2.0
Constants: 2.2.1
Muons: 1.1

Table 1. Sample locations and basin characteristics

Sample ID	Latitude (degrees)	Longitude (degrees)	Area (km^2)	%BRE	Province	Relief (meters)	Mean Slope (°) (degrees)	Median Slope (°) (degrees)	Mean Elevation (meters)	Effective Elevation (meters)
CS-01	36.6206	-80.7778	1.98	6	BR	93	5.7	5	868	868
CS-02	36.4478	-80.8480	2.75	52	BRE	191	7.7	7	478	478
CS-03	36.4683	-80.8305	89.57	62	BRE	662	11.1	9	548	558
CS-04	36.4747	-80.8572	0.89	100	BRE	238	14.8	14	503	505
CS-05	36.4750	-80.8572	4.06	78	BRE	269	9.6	8	475	475
CS-06	36.5391	-80.8583	0.64	100	BRE	364	17.8	18	598	601
CS-07	36.5611	-80.7995	1.20	98	BRE	600	19.4	18	744	754
CS-08	36.5170	-80.7911	3.76	6	BR	154	5.8	5	857	857
CS-09	35.3335	-82.3925	3.78	0	BR	91	4.5	4	686	687
CS-10	35.3578	-82.4050	0.81	0	BR	107	10	10	711	711
CS-11	35.3210	-82.3242	18.11	83	BRE	522	12.1	11	807	810
CS-12	35.2859	-82.2911	5.07	100	BRE	571	16.8	16	642	649
CS-13	35.3133	-82.2189	3.14	49	PIED	268	9.5	8	388	390
CS-14	35.2942	-82.2331	0.63	100	BRE	518	20.9	20	590	599
CS-15	35.3425	-82.1818	16.99	51	BRE	722	11.7	10	458	467
CS-16	35.5419	-82.3828	11.27	0	BR	569	15	15	888	892
CS-17	35.5489	-82.3113	7.36	82	BRE	513	17.2	17	1028	1033
CS-18	35.5236	-82.3311	3.07	0	BR	389	12.4	12	814	816
CS-19	35.6361	-82.2178	6.83	100	BRE	520	18.9	19	707	712
CS-20	35.6253	-82.1761	35.83	89	BRE	655	14.8	15	678	686
CS-21	35.5848	-82.1606	47.67	68	BRE	624	12.5	11	594	599
CS-22	35.5692	-82.2147	11.01	100	BRE	573	16.1	15	719	723
CS-23	35.5244	-82.1678	4.32	100	BRE	548	15.4	15	679	682
CS-24	35.5455	-82.4053	5.34	0	BR	609	17.2	18	1044	1051
CS-25	36.7172	-80.4313	5.12	0	BR	175	6.5	6	904	904
CS-26	36.7727	-80.4625	4.93	0	BR	390	11.7	11	923	925
CS-27	36.7533	-80.3731	8.47	29	BR	159	6.7	6	951	952
CS-28	36.7856	-80.2980	6.01	100	BRE	546	15.4	15	618	623
CS-29	36.7275	-80.2253	18.18	85	BRE	548	13.4	12	565	568
CS-30	36.6537	-80.1800	4.51	1	PIED	194	5.8	5	427	428
CS-31	36.6655	-80.3384	5.56	100	BRE	400	18.3	19	690	694
CS-32	36.6142	-80.4505	4.01	100	BRE	449	17.7	17	564	569
CSB-1	36.6200	-80.7600							892	
CSB-2	35.4300	-82.2500							694	
CSB-3	35.6200	-82.2600							957	

CS samples are fluvial sediment; CSB samples are bedrock outcrops; BRE = Blue Ridge Escarpment; BR = Blue Ridge; PIED = Piedmont.
%BRE indicates percent of basin area draining the Blue Ridge Escarpment as defined in the text
Province indicates which province (by area) dominates the drainage basin.
Elevation is mean basin elevation; Effective elevation is used in CRONUS erosion rate calculation following Portenga and Bierman (2011)

10.71 avg 17.57878358
5.00 median

Table 2. Cosmogenic nuclide data and erosion rates

Sample ID	Grain Size (mm)	^{9}Be Carrier (µg)	Quartz (g)	AMS ID#	Blank corrected ^{10}Be/^{9}Be (x 10^{-13})	Measured ^{10}Be (atoms/g)	Erosion rate (m/Ma)							
CS-01	0.25-0.85	304	37.13	BE22565	11.80 ± 0.20	644000 ± 11100	10.0 ± 0.8	1.18E-12	±	2.03E-14	1			
CS-01	0.85-2	305	39.27	BE22566	13.80 ± 0.27	716000 ± 13900		1.38E-12	±	2.67E-14	2			
CS-01	2-9	304	40.09	BE22567	13.30 ± 0.27	675000 ± 13700		1.33E-12	±	2.70E-14	3			
CS-01	>9	303	35.36	BE22568	19.50 ± 0.39	1110000 ± 22400		1.95E-12	±	3.91E-14	4			
CS-02	0.25-0.85	300	40.93	BE22581	10.50 ± 0.25	512000 ± 12000	9.6 ± 0.8	1.05E-12	±	2.46E-14	5			
CS-02	0.85-2	307	40.06	BE22582	9.77 ± 0.17	500000 ± 8700		9.77E-13	±	1.70E-14	6			
CS-02	2-9	299	40.02	BE22583	9.20 ± 0.16	459000 ± 8010		9.20E-13	±	1.60E-14	7			
CS-02	>9	306	39.40	BE22584	12.00 ± 0.27	625000 ± 13800		1.20E-12	±	2.66E-14	8			
CS-03	0.25-0.85	303	32.80	BE22569	6.04 ± 0.15	373000 ± 9010	14.5 ± 1.1	6.04E-13	±	1.46E-14	9			
CS-03	0.85-2	304	37.83	BE22570	6.85 ± 0.17	368000 ± 8860		6.85E-13	±	1.65E-14	10			
CS-03	2-9	300	40.11	BE22571	6.49 ± 0.16	324000 ± 7770		6.49E-13	±	1.56E-14	11			
CS-03	>9	303	40.06	BE22585	8.62 ± 0.15	436000 ± 7620		8.62E-13	±	1.51E-14	12			
CS-04	0.25-0.85	252	22.44	BE22533	4.39 ± 0.11	330000 ± 8410	16.0 ± 1.2	4.39E-13	±	1.12E-14	13			
CS-04	0.85-2	253	29.74	BE22534	6.07 ± 0.15	344000 ± 8290		6.07E-13	±	1.46E-14	14			
CS-04	2-9	252	31.27	BE22535	5.59 ± 0.14	301000 ± 7270		5.59E-13	±	1.35E-14	15			
CS-04	>9	252	33.61	BE22536	6.19 ± 0.13	310000 ± 6620		6.19E-13	±	1.32E-14	16			
CS-05	0.25-0.85	252	40.10	BE22586	9.45 ± 0.23	480000 ± 11800	10.3 ± 0.8	9.45E-13	±	2.33E-14	17			
CS-06	0.25-0.85	251	40.69	BE22541	5.81 ± 0.09	239000 ± 3510	24.3 ± 1.7	5.81E-13	±	8.53E-15	18			
CS-06	0.85-2	253	40.15	BE22542	5.22 ± 0.13	220000 ± 5400		5.22E-13	±	1.28E-14	19			
CS-06	2-9	253	24.84	BE22543	3.31 ± 0.07	225000 ± 5100		3.31E-13	±	7.49E-15	20			
CS-06	>9	253	20.61	BE22544	3.24 ± 0.07	266000 ± 5680		3.24E-13	±	6.93E-15	21			
CS-07	0.25-0.85	303	29.74	BE22549	7.06 ± 0.18	481000 ± 12400	12.6 ± 1.0	7.06E-13	±	1.82E-14	22			
CS-07	0.85-2	301	24.17	BE22550	4.27 ± 0.11	355000 ± 9450		4.27E-13	±	1.14E-14	23			
CS-07	2-9	302	23.66	BE22551	3.37 ± 0.09	287000 ± 7810		3.37E-13	±	9.17E-15	24			
CS-07	>9	307	31.13	BE22552	3.76 ± 0.07	248000 ± 4400		3.76E-13	±	6.69E-15	25			
CS-08	0.25-0.85	314	24.47	BE22587	7.96 ± 0.19	682000 ± 16200	9.3 ± 0.8	7.96E-13	±	1.89E-14	26			
CS-09	0.25-0.85	311	28.26	BE23185	4.28 ± 0.09	416000 ± 8670	13.9 ± 1.1	4.28E-13	±	8.92E-15	27			
CS-10	0.25-0.85	308	26.98	BE23186	3.74 ± 0.08	378000 ± 8190	15.6 ± 1.2	3.74E-13	±	8.10E-15	28			
CS-11	0.25-0.85	244	20.48	b2276	4.47 ± 0.10	356000 ± 8320	17.6 ± 1.4	4.47E-13	±	1.04E-14	29			
CS-12	0.25-0.85	247	22.18	b2277	3.39 ± 0.11	252000 ± 8500	23.0 ± 1.8	3.39E-13	±	1.14E-14	30			
CS-13	0.25-0.85	305	25.01	BE23187	3.13 ± 0.12	339000 ± 12500	14.1 ± 1.2	3.13E-13	±	1.15E-14	31	averaged replicates		
CS-14	0.25-0.85	304	34.74	BE23189	2.06 ± 0.06	121000 ± 3610	49.2 ± 3.6	2.06E-13	±	6.15E-15	32			
CS-14 (rep)	0.25-0.85	315	24.34	b2278	1.84 ± 0.06	124000 ± 4000	47.6 ± 3.5	1.84E-13	±	5.94E-15	33	48.4	1.145512986	3.6
CS-15	0.25-0.85	303	34.67	BE23190	5.49 ± 0.11	321000 ± 6490	15.8 ± 1.2	5.49E-13	±	1.11E-14	34			
CS-16	0.25-0.85	303	40.10	BE23191	8.37 ± 0.16	422000 ± 8070	15.8 ± 1.2	8.37E-13	±	1.60E-14	35			
CS-17	0.25-0.85	248	10.57	b2279	2.27 ± 0.07	355617 ± 10500	20.7 ± 1.6	2.27E-13	±	6.69E-15	36			
CS-18	0.25-0.85	304	31.82	BE23192	8.03 ± 0.15	513000 ± 9840	12.1 ± 0.9	8.03E-13	±	1.54E-14	37			
CS-19	0.25-0.85	304	30.35	BE23193	2.81 ± 0.07	188000 ± 4960	33.3 ± 2.5	2.81E-13	±	7.42E-15	38			
CS-20	0.25-0.85	303	26.45	BE23213	2.76 ± 0.09	211000 ± 6570	29.0 ± 2.2	2.76E-13	±	8.59E-15	39			
CS-21	0.25-0.85	309	40.90	BE23194	4.96 ± 0.10	251000 ± 5160	22.7 ± 1.7	4.96E-13	±	1.02E-14	40			
CS-22	0.25-0.85	304	29.06	BE23208	2.82 ± 0.08	197000 ± 5460	31.9 ± 2.4	2.82E-13	±	7.81E-15	41			
CS-23	0.25-0.85	306	40.02	BE23195	4.32 ± 0.23	221000 ± 11800	27.5 ± 2.4	4.32E-13	±	2.30E-14	42			
CS-24	0.25-0.85	303	25.00	BE23214	2.78 ± 0.07	226000 ± 5890	34.1 ± 2.6	2.78E-13	±	7.25E-15	43			
CS-24 (rep)	0.25-0.85	247	22.64	b2280	3.51 ± 0.10	256000 ± 7010	29.6 ± 2.3	3.51E-13	±	9.60E-15	44	31.9	3.23147799	2.4
CS-25	0.25-0.85	307	35.91	BE23197	13.30 ± 0.50	761000 ± 28500	8.5 ± 0.8	1.33E-12	±	4.98E-14	45			
CS-26	0.25-0.85	303	20.03	BE23215	6.36 ± 0.14	643000 ± 13900	10.4 ± 0.8	6.36E-13	±	1.37E-14	46			
CS-27	0.25-0.85	306	32.03	BE23209	10.60 ± 0.30	680000 ± 19300	10.0 ± 0.8	1.06E-12	±	3.01E-14	47			
CS-28	0.25-0.85	304	21.64	BE23210	3.53 ± 0.10	331000 ± 9210	17.4 ± 1.3	3.53E-13	±	9.82E-15	48			
CS-29	0.25-0.85	301	38.42	BE23198	13.50 ± 0.26	704000 ± 13770	7.2 ± 0.6	1.35E-12	±	2.64E-14	49			
CS-30	0.25-0.85	304	40.05	BE23199	9.53 ± 0.47	483000 ± 23700	9.9 ± 0.9	9.53E-13	±	4.67E-14	50			
CS-30 (rep)	0.25-0.85	247	19.74	b2283	5.60 ± 0.29	459390 ± 24100	10.4 ± 1.0	5.60E-13	±	2.88E-14	51	10.2	0.325269119	0.9
CS-31	0.25-0.85	307	32.12	BE23200	2.84 ± 0.08	181000 ± 5330	34.8 ± 2.6	2.84E-13	±	8.37E-15	52			
CS-32	0.25-0.85	306	34.91	BE23211	4.60 ± 0.11	269000 ± 6260	20.9 ± 1.6	4.60E-13	±	1.07E-14	53			
CSB-1	NA	304	26.40	BE23201	0.89 ± 0.05	68800 ± 4030	106.3 ± 9.5	8.94E-14	±	5.24E-15	54			
CSB-2	NA	303	13.08	BE23216	17.50 ± 0.35	2710000 ± 54800	1.5 ± 0.2	1.75E-12	±	3.54E-14	55			
CSB-3	NA	303	28.71	BE23202	4.73 ± 0.17	334000 ± 11900	20.8 ± 1.7	4.73E-13	±	1.68E-14	56			

1. Analytic uncertainty is one standard deviation. Samples run at Livermore National Laboratory (BE #) were normalized to KNSTD3110 with assumed ratio of 3150 x 10^{-15}. Samples run at SUERC (b#) were normalized to NIST standard with assummed ratio of 30600 x 10^{-15}

2. Measured ratios were corrected for process blanks run with each batch of samples and the uncertainty was propagated in quadrature. Process blanks (n=10) for samples prepared at the University of Vermont and analyzed at Livermore National Laboratory (BE#) averaged 2.1±0.3 x 10^{-14}. A single process blank for samples prepared and analyzed at SUERC (b #) returned a ratio of 1.1±0.1 x 10^{-14}. Blank corrections were applied specifally for samples measured on the different accelorators.

3. Erosion rates calculated using CRONUS (Balco et al., 2008); Wrapper script: 2.2, Main calculator: 2.1, Objective function: 2.0, Constants: 2.2.1, Muons: 1.1; global production rate and Lal/Stone scaling with no geomagnetic forcing. External uncertainty reported at one standard deviation.

	10.6	min	121000.0	min	7.2
max	40.9	max	1110000.0	max	49.2

Table 3. Summary of measured and modeled erosion rates

					Erosion rate (m/Ma)			Erosion/slope relationship		
Province	Average slope, sampled basins	# basins sampled	Average slope, modelled basins	# modeled basins	Arithmetic average of sampled basins	Area-weighted average of sampled	Area-weighted average of modelled basins (regression model)	Regression slope	Regression intercept	Correlation coefficient (R^2)
Blue Ridge	9.6±4.4	10	13.3±4.3	447	13.7	14.1	18.0	1.132	2.933	0.52
Escarpment	15.1±3.5	20	14.3±2.6	145	21.9	19.6	20.5	1.959	-7.666	0.46
Piedmont	7.7±2.6	2	6.2±2.7	492	12.2	11.8	9.9	1.060	4.015	1.00

Modelled basins defined using GIS as described in the text. Erosion rate/slope relationship modelled using linear regression. Uncertainty is one standard deviation around the mean.

Mean Slope ('	Blue Ridge	Escarpment	Piedmont
5.7	10		
10	15.6		
15	15.8		
5.8	9.3		
12.4	12.1		
6.7	10		
17.2	31.9		
6.5	8.5		
4.5	13.9		
11.7	10.4		
7.7		9.6	
19.4		12.6	
14.8		16	
17.8		24.3	
11.7		15.8	
11.1		14.5	
17.2		20.7	
9.6		10.3	
18.9		33.3	
14.8		[illegible]	
12.5		[illegible]	
16.1		[illegible]	
15.4		27.5	
12.1		17.6	
16.8		[illegible]	
20.9		[illegible]	
15.4		[illegible]	
13.4		[illegible]	
18.3		[illegible]	
17.7		[illegible]	
9.5			14.1
5.8			10.2
	48.4	max	
	7.2	min	

	average erosion rate	1sem erosion	average basin slope	1 sem slope	1 SD slope	n
blue ridge	13.8	2.2	9.55	1.39	4.38	10
peidmont	12.2	2.0	7.65	1.85	2.62	2
escarpment	21.9	2.3	15.08	0.78	3.48	20

f(v) = 1.345620E+0*v + 1.447793E+0
R^2 = 9.910526E-1

Blue Ridge	Escarpment	Piedmont			
4.5		9.55	4.3841254		
5.7					
5.8					
6.5					
6.7					
10					
11.7					
12.4					
15					
17.2					
	7.7	15.08	3.48479404		
	9.6				
	11.1				
	11.7				
	12.1				
	12.5				
	13.4				
	14.8				
	14.8				
	15.4				
	15.4				
	16.1				
	16.8				
	17.2				
	17.7				
	17.8				
	18.3				
	18.9				
	19.4				
	20.9				
		9.5		7.65	2.61629509
		5.8			

thse are mean basin slopes sampled